Geochimica et Cosmochimica Acta 369 (2024) 17–34

Contents lists available at ScienceDirect

Geochimica et Cosmochimica Acta

journal homepage: www.elsevier.com/locate/gca

Iron isotope fractionation during sulfide-promoted reductive dissolution of iron (oxyhydr)oxide minerals

Alison McAnena [a,1], Silke Severmann [b], Romain Guilbaud [c], Simon W. Poulton [d,*]

[a] School of Civil Engineering and Geosciences, Newcastle University, Drummond Building, Newcastle upon Tyne NE1 7RU, UK
[b] Department of Marine and Coastal Sciences, 71 Dudley Rd., Rutgers University, New Brunswick, NJ 08901, USA
[c] CNRS, Géosciences Environnement Toulouse, UMR5563, 31400 Toulouse, France
[d] School of Earth and Environment, University of Leeds, Leeds, LS2 9JT, UK

ARTICLE INFO

Associate editor: Weiqiang Li

Keywords:
Reductive dissolution
Iron oxides
Sulfide
Iron isotopes

ABSTRACT

Iron isotopes are a valuable tool for evaluating processes that control Fe redox cycling in modern and ancient environmental settings. However, robust evaluation of Fe isotope compositions in natural samples requires that fractionations associated with key (bio)geochemical reactions are well-defined. The reductive dissolution of Fe (oxyhydr)oxide minerals mediated by dissolved sulfide exerts a major influence on solid phase Fe mineralogy and dissolved porewater Fe profiles during early diagenesis of organic-rich sediments, but to date, no studies have investigated Fe isotope fractionations during this process. Here, we report the results of laboratory sulfidation experiments, examining apparent Fe isotope fractionations for a variety of Fe (oxyhydr)oxide minerals. The iron isotope compositions of reaction products were determined for both the reduction-dominated and dissolution-dominated steps of the reaction. The reductive step for lepidocrocite and hematite produced Fe(II) that was up to 0.25 ‰ heavier than the bulk starting mineral. By contrast, the reduction of ferrihydrite produced isotopically light Fe(II), with isotope compositions −0.1 to −0.6 ‰ lower than the initial mineral. Consistent with previous studies of the reductive dissolution of Fe (oxyhydr)oxide minerals via abiological and biological pathways, the lighter isotope was preferentially released from the mineral surface during the dissolution phase for all minerals, with dissolved Fe^{2+} isotope compositions up to ~2.0 ‰ lower than the surface bound Fe(II). The magnitude of isotopic fractionation during both of these steps is directly related to rates of reaction, and is thus controlled by factors such as sulfide concentration, mineral concentration, crystal structure, surface area and pH. Our data demonstrate that dissolved Fe^{2+} with $\delta^{56}Fe$ compositions approaching −1.0 ‰ is readily generated during the overall reaction, suggesting that sulfide-promoted reductive dissolution of Fe (oxyhydr)oxide minerals may contribute significantly to the generation of light Fe isotope compositions in anoxic settings.

1. Introduction

Over the last twenty years, iron (Fe) isotopes have emerged as a powerful tool for evaluating Fe biogeochemical cycling in modern and ancient marine environments (e.g., Dauphas and Rouxel, 2006; Johnson et al., 2008a). However, the task of deciphering the relative roles of different potential fractionation pathways in specific settings is not trivial (Anbar, 2004; Rouxel et al., 2005, 2008; Yamaguchi et al., 2005; Czaja et al., 2010, 2012; Guilbaud et al., 2012; Heard et al., 2020). In large part, the uncertainty relates to the complexity of environmental reactions, both biological and abiological, in which Fe plays a central role, and where associated Fe isotope fractionations are of comparable magnitude. Therefore, it is necessary to understand both the dominant Fe cycling pathways and their isotope fractionations in order to interpret Fe isotope signatures.

The largest Fe isotope fractionations (between 2 ‰ and 12 ‰) occur in association with changes in oxidation state (e.g., Johnson et al., 2002; Welch et al., 2003; Crosby et al., 2005; Balci et al., 2006; Wiederhold et al., 2006; Crosby et al., 2007; Beard et al., 2010; Kappler et al., 2010; Wu et al., 2012b; Amor et al., 2016; Oleinikova et al., 2019) and bonding environment (e.g., Matthews et al., 2001; Icopini et al., 2004; Teutsch et al., 2005; Guilbaud et al., 2011a; Ilina et al., 2013), and tend to be best expressed in natural environments where significant quantities of Fe may be mobilised and transported away from the initial reaction site

* Corresponding author.
E-mail address: s.poulton@leeds.ac.uk (S.W. Poulton).
[1] Current address: Office for the Vice Provost for Research, Innovation and Global Engagement, University College London, London, WC1E 6BT, UK.

https://doi.org/10.1016/j.gca.2024.01.032
Received 27 June 2022; Accepted 29 January 2024
Available online 3 February 2024

(see Severmann et al., 2006; Johnson et al., 2008b; Scholz et al., 2014a, b). Both biological and abiological experimental studies suggest that the largest fractionations occur during bacterial Fe(II) photo-oxidation (Croal et al., 2004; Balci et al., 2006; Kappler et al., 2010; Amor et al., 2016), dissimilatory iron reduction (DIR) (Beard et al., 1999, 2003; Icopini et al., 2004; Crosby et al., 2005, 2007; Johnson et al., 2005; Wu et al., 2009; Tangalos et al., 2010; Chanda et al., 2021), and rapid pyrite formation (Guilbaud et al., 2011a; Rolison et al., 2018). Other abiotic, non-redox precipitation pathways tend to produce more modest fractionations (<2 ‰) (Skulan et al., 2002; Wiesli et al., 2004; Butler et al., 2005; Guilbaud et al., 2010, 2011b; Wu et al., 2012a; Mansor and Fantle, 2019).

Weathering and non-DIR dissolution processes tend to be accompanied by smaller fractionations that produce isotopically light dissolved $Fe_{(aq)}$ with respect to the bulk mineral (Brantley et al., 2001, 2004; Fantle and DePaolo, 2004; Wiederhold et al., 2006; Chapman et al., 2009; Kiczka et al., 2010; Liermann et al., 2011; Wolfe et al., 2016; Opfergelt et al., 2017; Mulholland et al., 2021; Maters et al., 2022; Qi et al., 2022). In terms of abiotic pathways, studies have mainly focussed on proton- and ligand-promoted mineral dissolution. For instance, dissolution of goethite by oxalate (for both reductive and non-reductive mechanisms) is reported to produce a significant kinetic isotope fractionation, with an aqueous phase 1.7 ‰ lighter than the starting oxide mineral during the early stages of dissolution (Wiederhold et al., 2006). These ligand-promoted fractionation values contrast with other non-reductive proton-promoted dissolution fractionations (via 0.5 M HCl), whereby no fractionation was observed for oxide dissolution (Wiederhold et al., 2006). Thus, there is clearly potential for significant fractionations in nature due to organic ligand chelation (see also Kiczka et al., 2010; Liermann et al., 2011). However, although oxalate is an important organic ligand in nature that plays a substantial role in mineral weathering (e.g., Drever and Stillings, 1997), it is not a particularly significant reductant in the marine environment. A far more important reductive process relates to the generation of dissolved sulfide by microbial sulfate reduction (MSR). Sulfide formed by this process can take part in a variety of reactions, ultimately leading to the formation of pyrite (FeS_2), with mackinawite (FeS) as a common intermediate phase (Berner, 1984; Benning et al., 2000; Rickard and Morse, 2005).

Iron isotope fractionations during the formation of FeS, $FeS^0_{(aq)}$, $FeSH^+$ and FeS_2 from dissolved Fe^{2+} (i.e., abiological reactions involving no Fe redox change) have been examined in marine and lacustrine sediments (Severmann et al., 2006; Busigny et al., 2014; Rolison et al., 2018), as well as in a number of laboratory studies (Butler et al., 2005; Guilbaud et al., 2010, 2011a, b; Wu et al., 2012a; Mansor and Fantle, 2019). During rapid precipitation of FeS, the lighter isotope is preferentially incorporated into the mineral phase, with an initial kinetic isotope fractionation between FeS and $Fe^{2+}_{(aq)}$ of –0.85 ± 0.30 ‰, while fractionations become smaller after aging of the FeS for several days (Butler et al., 2005; Guilbaud et al., 2010). In fact, under circumneutral and alkaline conditions, atom exchange might continue towards isotopic equilibrium, where FeS becomes isotopically heavier than $Fe^{2+}_{(aq)}$ (Guilbaud et al., 2011b; Wu et al., 2012a). Additional fractionation favouring the lighter isotope in the mineral phase then occurs during partial pyritization of FeS, with the effect that, theoretically, abiotic formation of pyrite has the potential to produce fractionations spanning almost the entire range of signatures observed in natural samples (Guilbaud et al., 2011a; Busigny et al., 2014; Scholz et al., 2014b; Rolison et al., 2018; Mansor and Fantle, 2019; Ostrander et al., 2022; Dupeyron et al., 2023).

Such studies highlight the need for careful consideration of the geochemical characteristics of individual samples when evaluating potential processes controlling Fe isotope fractionations in nature. Importantly, however, sulfide produced by MSR also reacts directly with Fe (oxyhydr)oxide minerals, resulting in reductive dissolution of the Fe mineral and oxidation of the sulfide (Rickard, 1974; Pyzik and Sommer, 1981; Dos Santos and Stumm, 1992; Peiffer et al., 1992; Yao and Millero, 1996; Poulton, 2003; Poulton et al., 2004). This reaction has been suggested to be dominant over DIR in many organic-rich marine sediments, ultimately leading to the release of $Fe(II)_{aq}$ to porewaters, and subsequently the formation of FeS and pyrite (Canfield, 1989; Krom et al., 2002).

Although Fe isotope fractionation during sulfide-mediated reductive dissolution of Fe (oxyhydr)oxide minerals has been recognised as a potentially important process affecting modern and ancient marine sediments during early diagenesis (e.g., Archer and Vance, 2006; Severmann et al., 2006; Staubwasser et al., 2006; Roy et al., 2012), no experimental studies have yet been performed to evaluate this possibility. Here, we report Fe isotope data for experiments examining Fe isotope fractionations during sulfide-promoted reductive dissolution of a range of Fe (oxyhydr)oxide minerals. In addition to reporting bulk dissolution isotopic signatures, we also investigate how different stages of the reaction mechanism affect fractionations, with an overall aim to enhance our ability to evaluate process controls on sedimentary Fe isotope signatures in modern and ancient settings.

2. Sulfide-promoted reductive dissolution mechanism and kinetics

The pathway by which a variety of Fe (oxyhydr)oxide minerals (e.g., ferrihydrite, goethite, hematite, lepidocrocite, magnetite) undergo sulfide-promoted reductive dissolution is reasonably well-defined (Rickard, 1974; Pyzik and Sommer, 1981; Dos Santos and Stumm, 1992; Peiffer et al., 1992; Yao and Millero, 1996; Poulton, 2003; Poulton et al., 2004), and can be simplified to:

Surface complexation:

$$>Fe^{III}OH + HS^- \leftrightarrow >Fe^{III}S^- + H_2O \quad (1)$$

Electron transfer:

$$>Fe^{III}S^- \leftrightarrow >Fe^{II}S \quad (2)$$

Release of the oxidized product:

$$>Fe^{II}S + H_2O \leftrightarrow >Fe^{II}(OH)^+_2 + S^{\bullet -} \quad (3)$$

Detachment of Fe(II):

$$>Fe^{II}(OH)^+_2 \rightarrow \text{free surface site} + Fe^{2+} \quad (4)$$

The overall process describes the initial formation of a sulfide complex (Eq. (1)) on the reactive surface of an Fe(III) oxide mineral, followed by rapid electron transfer (Eq. (2)) between Fe(III)-Fe(II) and the release of an $S^{\bullet -}$ radical (Eq. (3)) to solution. The rate limiting step is determined by the release of Fe(II) to solution (Eq. (4)) (Dos Santos and Stumm, 1992); at circumneutral pH and above, Fe(II) can remain associated with the oxide surface for considerable periods of time, dependent on the mineralogy of the oxide (Poulton, 2003; Poulton et al., 2004). This (oxyhydr)oxide-associated Fe(II) pool is represented by $>Fe^{II}S$ and $>Fe^{II}(OH)^+_2$ in Eqs. (2)–(4) (which we hereafter refer to as $Fe(II)_{ox}$), and is distinct from any Fe(II) that may have been re-adsorbed at the mineral surface. There have been few studies focusing on the mineralogical characterisation of $Fe(II)_{ox}$. In addition to the surficial $>Fe^{II}(OH)^+_2$ species described by several authors (e.g., Pyzik and Sommer, 1981; Poulton, 2003), there is high-resolution TEM evidence for extensive formation of an FeS rim covering lepidocrocite crystals at circumneutral pH, with magnetite as an intermediate phase at the lepidocrocite-FeS boundary (Hellige et al., 2012). In fact, the presence of magnetite intermediates confirms that electron transfer may reach the bulk mineral instead of being restricted to its surface (Zinder et al., 1986; Yanina and Rosso, 2008; Handler et al., 2009).

Furthermore, the free $S^{\bullet -}$ radical will rapidly reduce Fe(III) ions at the oxide surface to form a higher oxidation state S species (e.g., elemental S; Eq. (5)) (Pyzik and Sommer, 1981; Yao and Millero, 1996; Poulton, 2003; Poulton et al., 2004):

$$8{>}FeOH + 8S^{\bullet -} \rightarrow S_8^0 + 8Fe^{2+} \quad (5)$$

Following dissolution, $Fe^{2+}_{(aq)}$ can then react rapidly with sulfide remaining in solution to form FeS (Eq. (6)):

$$Fe^{2+} + HS^- \leftrightarrow FeS + H^+ \quad (6)$$

Consequently, theoretically, for each mole of FeS formed, one mole of HS^- is consumed during reductive dissolution and a further mole of HS^- is consumed during reaction with free $Fe^{2+}_{(aq)}$. However, this ratio will vary due to the formation of both elemental sulfur and polysulfide, as demonstrated by X-ray photoelectron spectroscopy for the sulfidation of both goethite and lepidocrocite (Wan et al., 2014).

Poulton et al. (2004) presented a reactivity scheme for the reductive dissolution of a variety of Fe (oxyhydr)oxide minerals towards dissolved sulfide. At circumneutral pH, minerals with a lower degree of crystal order (ferrihydrite and lepidocrocite) are reactive on a time-scale of minutes to hours, while more ordered minerals (goethite, hematite and magnetite) are reactive on a time-scale of tens of days. Thus, mineralogical properties associated with the crystal structure, such as bonding environment, relative surface area and the concentration of reactive surface sites, all affect the relative reactivities of different minerals. In addition, factors such as pH exert a strong control on dissolution rates, and in particular this controls the rate at which $Fe(II)_{ox}$ is released to solution (Yao and Millero, 1996; Poulton, 2003; Poulton et al., 2004). Therefore, all of these factors have the potential to lead to variability in the extent of Fe isotope fractionation for different minerals.

3. Materials and methods

3.1. Synthesis of iron minerals

All Fe minerals were prepared according to the methods of Schwertmann and Cornell (1991). Two-line ferrihydrite was synthesised by adjusting the pH of a 0.1 M $Fe(NO_3)_3{\cdot}9H_2O$ solution to 7.5 via addition of 1 M KOH. Goethite (α-FeOOH) was synthesised from a solution containing 1 M $Fe(NO_3)_3$ and 5 M KOH, which was heated at 70 °C for 60 h. Hematite (Fe_2O_3) was produced by heating a solution of 0.02 M $Fe(NO_3)_3{\cdot}9H_2O$ (dissolved in preheated 0.002 M HCl) for 7 days at 98 °C. Lepidocrocite (γ-FeOOH) was prepared by adjusting the pH of a 0.06 M $FeCl_2$ solution to pH 7 with NaOH, while slowly oxidising Fe(II) via the addition of $O_{2(g)}$. Iron mineralogy was confirmed by X-ray Diffraction (XRD; Philips X'Pert PANalytical). The surface area of each mineral was determined using multi-point Brunauer-Emmett-Teller (BET) surface area analysis (Gemini 2375 V4.02) following degassing overnight at room temperature, giving values of 184 m^2/g, 128 m^2/g, 35 m^2/g and 2.5 m^2/g for ferrihydrite, lepidocrocite, goethite and hematite, respectively.

3.2. Experimental

All solutions were prepared with de-ionised water which was deoxygenated with N_2 gas for at least one hour prior to use. Ultra-pure $N_{2(g)}$ (99.999 %) was further purified with an Agilent Technology O_2 trap and indicator. The experimental apparatus consisted of a 1 L glass reaction vessel with gas-tight induction ports to accommodate a pH electrode, a sample inlet/outlet valve, and a glass pipette for HCl addition (see Supplementary Material). A ~100 mM stock sulfide solution was prepared by dissolving $Na_2S{\cdot}9H_2O$ in N_2-purged water. Before addition, the $Na_2S{\cdot}9H_2O$ crystals were rapidly rinsed and dried to remove any oxidised surfaces from the solid (e.g., Poulton, 2003; Poulton et al., 2004).

Experiments were performed via addition of a known volume of stock sulfide solution to 1 L of deoxygenated 0.1 M NaCl, and the solution was stirred continuously within the reaction vessel. As the reaction consumes protons (e.g., Dos Santos and Stumm, 1992), deoxygenated HCl (0.001–0.1 M) was added via a Titralab TIM856 Titration Manager to maintain the required pH, with temperature within the vessel held at 25 °C using a 10 L heated water bath. Prior to starting the reaction, the initial concentration of dissolved sulfide was measured in triplicate (see below). A known weight of the Fe (oxyhydr)oxide mineral was then de-oxygenated (within a modified syringe attached to the input valve of the reaction vessel) and flushed into the sulfide solution as a 5 mL slurry, in either 0.01 M NaCl or, for experiments performed at higher pH, in di-Na tetraborate (at pH 8 or 8.5 to help maintain the initial pH in the reaction vessel immediately after addition of the mineral slurry). The direction of N_2 flow through the syringe was then switched and the input valve opened to force the de-oxygenated sample solution rapidly into the vessel. This process took less than 5 s and all ports remained closed, thus allowing the Fe (oxyhydr)oxide to be added to the reaction vessel under anoxic conditions (Poulton, 2003; Poulton et al., 2004). Full details of initial experimental conditions for each run are reported in Tables 1 and 2.

Experiments were conducted at low (4) and high (8–9) pH. Low pH experiments were specifically performed to minimize the concentration of FeS formed (where FeS is only a transient product of the sulfidation reaction due to enhanced solubility of FeS; Poulton, 2003; Rickard, 2006), and to give higher concentrations of dissolved $Fe(II)_{aq}$ ($Fe(II)_{aq}$ is dissolved from the mineral surface more rapidly at low pH; Poulton, 2003) in order to evaluate isotopic fractionations during the dissolution step of the reaction (Eqn. (4). Experiments at higher pH were performed in order to enhance the formation of $Fe(II)_{ox}$, to allow the reduction step of the reaction (Eq. (2)) to outcompete the dissolution step. Under these conditions, formation of free FeS (Eqn. (6) is minimised due to the relatively slow reaction kinetics of the dissolution step (Poulton, 2003). Iron isotope fractionations during formation of FeS have been reported previously (Butler et al., 2005; Guilbaud et al., 2010; 2011b; Wu et al., 2012a) and were not further investigated in our experiments.

In addition, a series of experiments were performed to investigate the possibility of isotopic zonation amongst the more ordered phases: synthetic goethite and hematite. Indeed, such zonations, with ^{56}Fe-enriched rims, have been observed in synthetic Fe (oxyhydr)oxides (e.g., Skulan et al., 2002). The minerals were digested in 6 M HCl for several hours until completely dissolved. Samples were taken every 20–60 mins during the dissolution and the Fe isotopic composition measured. Unfortunately, we were not able to perform this check on synthetic lepidocrocite and on ferrihydrite, due to the full consumption of our stock during the experiments. However, we note that for less ordered phases such as ferrihydrite, mineral zonation is not expected, as its expression demands well-ordered crystal structures. Furthermore, isotopic zonation has never been observed or documented for synthetic ferrihydrite (e.g., Bullen et al., 2001; Johnson et al., 2008b).

3.3. Chemical analyses

Samples for analysis of solid and dissolved phases were taken periodically by airtight syringe and analysed immediately. Dissolved sulfide (at our experimental pH range, $\Sigma S^{2-} \approx H_2S + HS^-$) was measured on 1 mL filtered (0.2 μm PTFE filters) samples and analysed spectrophotometrically using the methylene blue method (Cline, 1969). Total dissolved plus solid phase sulfide (FeS) was also measured via this technique using unfiltered samples (the methylene blue reagent is prepared in 50 % (v/v) HCl, resulting in the dissolution of FeS in the sample), and FeS was determined after subtraction of dissolved sulfide (see Yao and Millero, 1996; Poulton, 2003; Poulton et al., 2004). Replicate measurements of a stock sulfide solution gave a RSD of 4.5 % (n = 8). Total elemental sulfur was calculated as the difference between the initial sulfide concentration and the total sulfide concentration (solid plus dissolved) at a particular time.

Dissolved Fe^{2+} was measured on filtered samples by the ferrozine method (Viollier et al., 2000). Replicate measurements of a stock Fe(II) solution gave a RSD of 4.7 % (n = 8). Consistent with previous studies (Poulton, 2003; Poulton et al., 2004), values of $Fe(II)_{ox}$ were determined

Table 1
Initial experimental conditions, and chemical and isotopic data for experiments performed at pH 4. ΣFe(II)/Fe_T refers to the proportion (%) of the bulk mineral that has been reduced. Errors for isotope analysis are reported as 2σ. All isotope analyses are normalised to the bulk isotopic composition of each starting mineral. The isotope composition for the total combined Fe pools, δ56Fe_T, was calculated as the weighted sum of the three measured isotope pools. n.d. = not determined; n = number of analyses.

Experiment	Time (mins)	**Chemical data**					**Isotopic data**									
		$\Sigma S^{2-}_{(aq)}$ (μM)	$FeS_{(s)}$ (μM)	$Fe^{2+}_{(aq)}$ (μM)	Fe (II) ox (μM)	ΣFe (II)/Fe_T (%)	Fe^{2+}(aq)		n	δ^{56}Fe (‰)	$Fe(II)_{soli}$	n	Fe(III)unreac.		n	Fe_T (calculated)
							δ^{56}Fe (‰)	δ^{57}Fe (‰)			δ^{57}Fe (‰)		δ^{56}Fe (‰)	δ^{57}Fe (‰)		δ^{56}Fe (‰)
Ferrihydrite	0	212														
1.0g/L; pH 4	1	34	26	157	121	2.6	−0.15 ± 0.06	−0.19 ± 0.08	2	−0.20 ± 0.05	−0.182 ± 0.29	2	n.d.	n.d.		
	3	16	7	294	78	3.2	−0.23 ± 0.11	−0.32 ± 0.17	2	−0.063 ± 0.04	−0.049 ± 0.16	3	n.d.	n.d.		
	5	12	8	330	45	3.2	−0.18 ± 0.21	−0.34 ± 0.52	2	0.16 ± 0.10	0.24 ± 0.15	1	n.d.	n.d.		
	7	8	4	366	29	3.4	−0.16 ± 0.12	−0.22 ± 0.12	2	0.20 ± 0.01	0.45 ± 0.34	2	n.d.	n.d.		
	10	5	4	382	20	3.4	−0.10 ± 0.08	−0.15 ± 0.04	2	0.31 ± 0.04	0.46 ± 0.27	3	n.d.	n.d.		
	14	2	3	n.d.	n.d.		−0.08 ± 0.21	−0.20 ± 0.10	2	0.30 ± 0.02	0.43 ± 0.24	2	n.d.	n.d.		
	20	2	2	407	8	3.5	−0.13 ± 0.10	−0.20 ± 0.15	1	0.28 ± 0.14	0.35 ± 0.40	3	n.d.	n.d.		
	30	1	2	410	7	3.5	−0.16 ± 0.06	−0.22 ± 0.05	2	0.25 ± 0.14	0.32 ± 0.38	2	n.d.	n.d.		
	45	1	1	412	5	3.5	−0.10 ± 0.07	−0.24 ± 0.33	3	0.31 ± 0.04	0.53 ± 0.30	3	n.d.	n.d.		
	60	1	3	429	0	3.6	−0.12 ± 0.17	−0.19 ± 0.18	2	0.26 ± 0.08	0.36 ± 0.21	2	n.d.	n.d.		
Lepidocrocite	0	872														
0.25g/L; pH 4	1	730	0	38	246	10.1	0.34 ± 0.04	0.43 ± 0.13	3	0.28 ± 0.15	0.445 ± 0.34	2	0.023 ± 0.08	0.028 ± 0.11	3	0.05
	5	663	1	117	198	11.2	n.d.	n.d.		n.d.	n.d.		n.d.	n.d.		
	10	497	79	218	295	21.1	0.24 ± 0.04	0.38 ± 0.12	3	0.155 ± 0.02	0.244 ± 0.20	2	n.d.	n.d.		
	15	401	102	339	297	26.3	n.d.	n.d.		n.d.	n.d.		n.d.	n.d.		
	20	330	95	443	356	31.8	0.18 ± 0.06	0.27 ± 0.06	2	0.03 ± 0.16	0.04 ± 0.27	2	−0.02 ± 0.05	−0.01 ± 0.06	3	0.02
	30	258	118	627	247	35.3	n.d.	n.d.		n.d.	n.d.		n.d.	n.d.		
	45	208	103	876	143	36.4	0.06 ± 0.08	0.08 ± 0.11	3	0.03 ± 0.17	−0.08 ± 0.18	2	n.d.	n.d.		
	60	178	97	1050	47	42.5	n.d.	n.d.		n.d.	n.d.		n.d.	n.d.		
	90	149	63	n.d.	n.d.		0.05 ± 0.11	0.11 ± 0.12	5	0.07 ± 0.10	0.06 ± 0.15	1	n.d.	n.d.		
	180	105	4	1474	48	54.3	0.11 ± 0.06	0.17 ± 0.07	3	n.d.	n.d.		n.d.	n.d.		
Goethite	0	885														
0.5g/L; pH 4	1	747	35	18	153	3.7	−0.05 ± 0.06	−0.04 ± 0.27	4	0.16 ± 0.10	0.27 ± 0.07	2	−0.04 ± 0.07	−0.02 ± 0.17	2	−0.03
	7	722	38	85	125	4.4	n.d.	n.d.		n.d.	n.d.		n.d.	n.d.		
	15	677	38	185	115	6.0	0.15 ± 0.10	0.16 ± 0.21	2	0.40 ± 0.15	0.59 ± 0.13	2	n.d.	n.d.		
	25	632	38	294	96	7.6	n.d.	n.d.		n.d.	n.d.		n.d.	n.d.		
	45	571	40	443	46	9.4	0.29 ± 0.16	0.45 ± 0.30	3	0.53 ± 0.16	0.81 ± 0.21	3	−0.02 ± 0.06	−0.02 ± 0.16	4	0.01
	75	510	56	580	1	11.3	n.d.	n.d.		n.d.	n.d.		n.d.	n.d.		
	135	493	24	645	68	13.1	0.25 ± 0.10	0.36 ± 0.15	1	0.58 ± 0.02	0.77 ± 0.32	3	n.d.	n.d.		
	255	450	58	646	50	13.4	0.21 ± 0.01	0.27 ± 0.07	2	0.32 ± 0.18	0.53 ± 0.13	3	0.01 ± 0.20	0.06 ± 0.46	3	0.04
Hematite	0	1092														
0.5g/L; pH 4	1	1051	19	6	19	0.7	−0.33 ± 0.06	−0.49 ± 0.04	2	0.27 ± 0.10	0.34 ± 0.15	1	0.03 ± 0.03	0.06 ± 0.15	3	0.03
	10	1015	19	18	79	1.9	n.d.	n.d.		n.d.	n.d.		n.d.	n.d.		
	20	985	46	20	56	2.0	−0.51 ± 0.07	−0.79 ± 0.18	3	0.20 ± 0.10	0.31 ± 0.15	1	0.00 ± 0.13	0.01 ± 0.19	3	0.00
	75	942	47	31	128	3.3	−0.49 ± 0.10	−0.91 ± 0.15	1	0.29 ± 0.10	0.40 ± 0.15	1	n.d.	n.d.		
	135	929	37	37	178	4.0	n.d.	n.d.		n.d.	n.d.		n.d.	n.d.		
	195	913	31	41	224	4.7	−0.49 ± 0.22	−0.80 ± 0.57	2	0.36 ± 0.10	0.53 ± 0.15	1	n.d.	n.d.		
	255	888	61	44	181	4.6	n.d.	n.d.		n.d.	n.d.		n.d.	n.d.		
	315	854	66	47	231	5.5	−0.51 ± 0.20	−0.79 ± 0.33	3	n.d.	n.d.		n.d.	n.d.		

Table 2
Initial experimental conditions, and chemical and isotopic data for experiments performed at pH 8–9. $\Sigma Fe(II)/Fe_T$ refers to the proportion (%) of the bulk mineral that has been reduced. Errors for isotope analysis are reported as 2σ. All isotope analyses are normalised to the bulk isotopic composition of each starting mineral. The isotope composition for the total combined Fe pools, $\delta^{56}Fe_T$, was calculated as the weighted sum of the three measured isotope pools. n.d. = not determined; n = number of analyses.

Experiment	Time (mins)	**Chemical data**					**Isotopic data**										
		ΣS^{2-}(aq)	$FeS_{(s)}$	$Fe^{2+}_{(aq)}$	Fe(II)ox	$\Sigma Fe(II)/Fe_T$	Fe^{2+}(aq)		n	$\delta^{56}Fe$ (‰)	$Fe(II)_{solid}$		n	Fe(III)unreac		n	Fe_T (calculated)
		(μM)	(μM)	(μM)	(μM)	(%)	$\delta^{56}Fe$ (‰)	$\delta^{57}Fe$ (‰)			$\delta^{57}Fe$ (‰)			$\delta^{56}Fe$ (‰)	$\delta^{57}Fe$ (‰)		$\delta^{56}Fe$ (‰)
Ferrihydrite	0	291															
0.5g/L pH 8.5	1	160	2	4	108	1.9	−0.55 ± 0.10	−0.74 ± 0.15	1	−0.63 ± 0.10	−0.92	±0.15	1	n.d.	n.d.		
	3	124	20	4	126	2.5	−0.61 ± 0.10	−0.63 ± 0.15	1	−0.52 ± 0.01	−0.74	±0.08	2	n.d.	n.d.		
	5	118	13	4	159	3.0	−0.69 ± 0.27	−1.04 ± 0.22	2	−0.53 ± 0.02	−0.69	±0.23	2	n.d.	n.d.		
	10	91	13	5	212	3.9	n.d.	n.d.		−0.50 ± 0.20	−0.70	±0.30	3	n.d.	n.d.		
	20	51	16	6	282	5.1	−0.59 ± 0.10	−0.85 ± 0.13	2	−0.59 ± 0.20	−0.87	±0.35	3	n.d.	n.d.		
	30	21	12	6	354	6.3	−0.69 ± 0.06	−1.01 ± 0.17	2	−0.63 ± 0.09	−1.05	±0.36	4	n.d.	n.d.		
	40	5	10	5	393	6.9	n.d.	n.d.		n.d.	n.d.			n.d.	n.d.		
	60	0	1	5	430	7.4	n.d.	n.d.		n.d.	n.d.			n.d.	n.d.		
Ferrihydrite	0	863															
0.7g/L; pH 9.1	1	632	38	2	346	4.7	−0.73 ± 0.10	−1.13 ± 0.15	1	−0.43 ± 0.18	−0.61	±0.22	3	0.05 ± 0.19	0.11 ± 0.11	2	0.03
	5	520	53	2	525	7.0	n.d.	n.d.		n.d.	n.d.			n.d.	n.d.		
	10	463	64	3	605	8.1	−0.67 ± 0.08	−1.05 ± 0.25	2	−0.36 ± 0.23	−0.51	±0.35	3	n.d.	n.d.		
	20	400	53	3	764	9.9	n.d.	n.d.		n.d.	n.d.			n.d.	n.d.		
	30	346	79	5	792	10.6	n.d.	n.d.		−0.24 ± 0.14	−0.34	±0.19	2	0.07 ± 0.10	0.13 ± 0.05	2	
	45	279	83	6	913	12.1	n.d.	n.d.		n.d.	n.d.			n.d.	n.d.		
	60	235	41	6	1127	14.2	−0.59 ± 0.08	−0.86 ± 0.13	2	−0.23 ± 0.24	−0.32	±0.29	2	n.d.	n.d.		
	90	133	84	8	1200	15.6	n.d.	n.d.		n.d.	n.d.			n.d.	n.d.		
	120	102	88	10	1248	16.2	−0.68 ± 0.08	−0.98 ± 0.13	2	−0.15 ± 0.01	−0.25	±0.02	2	n.d.	n.d.		
	180	30	74	9	1435	18.3	n.d.	n.d.		n.d.	n.d.			n.d.	n.d.		
	240	19	64	n.d.	n.d.		−0.77 ± 0.02	−1.11 ± 0.01	2	−0.26 ± 0.03	−0.40	±0.03	2	0.05 ± 0.05	−0.03 ± 0.25	2	
Lepidocrocite	0	963															
0.3g/L; pH 8.6	1	957	0	0	12	0.4	n.d.	n.d.		0.12 ± 0.00	0.06	±0.06	3	−0.01 ± 0.05	−0.06 ± 0.18	3	
	5	911	5	0	89	2.8	n.d.	n.d.		n.d.	n.d.			n.d.	n.d.		
	10	888	11	0	117	3.8	n.d.	n.d.		0.14 ± 0.07	0.26	±0.11	4	n.d.	n.d.		
	20	852	26	1	143	5.0	0.37 ± 0.09	0.49 ± 0.20	3	n.d.	n.d.			n.d.	n.d.		
	30	814	34	2	194	6.8	0.14 ± 0.02	0.18 ± 0.03	2	0.16 ± 0.05	0.36	±0.19	4	−0.02 ± 0.07	−0.06 ± 0.01	4	−0.02
	60	685	47	3	412	13.7	0.09 ± 0.05	−0.01 ± 0.03	2	0.21 ± 0.09	0.34	±0.13	4	n.d.	n.d.		
	120	496	58	5	755	24.3	n.d.	n.d.		n.d.	n.d.			n.d.	n.d.		
	180	330	74	7	1037	33.2	0.02 ± 0.02	0.02 ± 0.07	2	0.17 ± 0.06	0.19	±0.15	5	n.d.	n.d.		
	240	150	93	8	1339	42.7	n.d.	n.d.		n.d.	n.d.			n.d.	n.d.		
	300	56	77	14	1569	49.2	0.05 ± 0.02	0.00 ± 0.17	2	0.20 ± 0.07	0.30	±0.08	4	−0.02 ± 0.07	−0.04 ± 0.06	4	0.08

by electron mass balance (after subtracting the measured concentrations of $Fe^{2+}_{(aq)}$ and FeS), since the total amount of Fe(II) produced (ΣFe(II)) can be estimated by doubling the concentration of oxidized sulfur at any point in time (Eq. (7)). While this is an approximation, since as discussed above, oxidised sulfur species were not measured directly, and the formation of polysulfides will consume a minor amount of the dissolved sulfide pool without oxidation (Wan et al., 2014), the isotopic mass balance calculated below (section 4.2) confirms that our approximation is valid.

$$2Fe^{3+} + HS^- \rightarrow 2Fe^{2+} + S^0 + H^+ \quad (7)$$

3.4. Iron isotope Analyses

At specific time intervals, 10 mL samples were taken for isotopic analysis of $Fe(II)_{aq}$, $Fe(II)_{solid}$ (which we define as the sum of $Fe(II)_{ox}$ + FeS), and unreacted Fe(III) (for selected samples). $Fe(II)_{aq}$ was collected via filtration (0.2 μm PTFE filters) into 100 μL of 10 % v/v HCl (to retain Fe in solution prior to analysis). A few drops of deoxygenated water were then immediately passed through the filter to remove any residual $Fe(II)_{aq}$, followed by 10 mL of 1 % v/v HCl to dissolve $Fe(II)_{ox}$ plus FeS, leaving only the remaining unreacted Fe(III) on the filter (see Poulton, 2003). Unfortunately, there is no way to chemically separate $Fe(II)_{ox}$ and FeS, since they are both readily dissolved by dilute acid. However, experiments were performed under conditions aimed at minimizing FeS precipitation, although as discussed below, this was a significant phase in some experiments. Finally, the filter was washed again and 10 mL of concentrated HCl was slowly passed through the filter into a third bottle to dissolve the remaining unreacted Fe(III). No coloured Fe mineral remained on the filter after this procedure, and extensive tests have demonstrated the effectiveness of these techniques for separating the different Fe phases (see Poulton, 2003; Poulton et al., 2004).

Samples for isotope analysis were processed through standard anion exchange chromatography following the protocol described in Beard et al. (2003). In brief, samples were dried down and re-dissolved in aliquots (0.2 mL) of 7 M HCl prior to loading onto 0.2 mL clean anion exchange resin. After removal of sample matrix with 4 mL of 7 M HCl, samples were eluted in 2 mL of 0.5 M HCl, dried down and converted to 2 % nitric acid matrix of 1–10 mg/L Fe concentration. The purified samples were spiked with equal amounts of Cu standard solution of known isotope composition (NIST-976 Cu isotope standard). Sample recovery was monitored using ferrozine analysis of samples before and after ion exchange chromatography, and only samples with >90 % recovery were used for isotope analysis. Iron isotope analyses were performed on a Thermo Scientific Neptune multi-collector inductively coupled plasma mass spectrometer (MC-ICP-MS) at the Woods Hole Oceanographic Institution (USA). Samples were introduced into the mass spectrometer as 0.2–2 mg/L Fe/Cu solutions, bracketed by standards of known isotope composition (typically international Fe isotope standard IRMM-14). Sample-standard-sample bracketing and simultaneous measurements of spiked Cu isotopes were used for mass bias correction. Mass-bias corrected isotope ratios of $^{56}Fe/^{54}Fe$ and $^{57}Fe/^{54}Fe$ are reported relative to the appropriate starting Fe mineral, using standard δ notation (in ‰):

$$\delta 56Fe = \left(\frac{56Fe/54Fe_{sample}}{56Fe/54Fe_{starting\ mineral}} - 1\right) \times 1000 \quad (8)$$

Several materials of known isotope composition, including SDO-1 (a black shale standard reference material with $\delta^{56}Fe = 0.036 \pm 0.046$ ‰ and $\delta^{57}Fe = 0.060 \pm 0.073$ ‰), BIR-1 (a basalt standard reference material with $\delta^{56}Fe = 0.051 \pm 0.046$ ‰ and $\delta^{57}Fe = 0.063 \pm 0.073$ ‰), and an in-house gravimetric standard (made by mixing IRMM-14 with ^{54}Fe-enriched tracer) were measured routinely for quality control. The average analytical precision (the repeatability of the analysis of internal standards during the analytical session) and the external precision (the repeatability of experimental triplicates) for $\delta^{56}Fe$ (2σ) are very similar at 0.13 ‰ and 0.10 ‰, respectively ($n = 3$), and analyses followed the expected mass-dependence.

4. Results

4.1. Chemical Speciation and Reaction Kinetics

The chemical speciation data for experiments performed at low and high pH (Table 1 and Fig. 1) are entirely consistent with previous studies (Poulton, 2003; Poulton et al., 2004). In order to account for rapid adsorption of sulfide at the oxide surface during the first minute after iron addition (see Poulton, 2003), initial dissolved sulfide was corrected using the back-extrapolation of polynomial data after t = 1 min. For the more reactive ferrihydrite, lepidocrocite and goethite minerals, the low pH experiments promoted rapid dissolution of $Fe(II)_{ox}$, leading to an increase in $Fe(II)_{aq}$ (Fig. 1a–c). By contrast, the low reactivity of hematite (see Poulton et al., 2004) led to slow dissolution rates, even at pH 4, and hence low concentrations of $Fe(II)_{aq}$ (Fig. 1D). Solid phase FeS dissolves readily at this pH (Rickard, 2006), and thus only persisted as a minor, transient product during the reaction (see Table 1). At pH 4, the solubility of FeS is dominated by the free hexaqua Fe^{2+} species (hereafter referred to as $Fe^{2+}_{(aq)}$; Rickard, 2006), and thus the speciation of $Fe(II)_{aq}$ produced during the low pH experiments largely consists of $Fe^{2+}_{(aq)}$. This is confirmed by speciation calculations in Phreeqc (Table S1), which indicate that 93–94 % of $Fe(II)_{aq}$ is characterized by $Fe^{2+}_{(aq)}$, for any starting mineral. As a result, $Fe^{2+}_{(aq)}$ was by far the most abundant reduced Fe species for the low pH experiments involving ferrihydrite, lepidocrocite and goethite, whereas $Fe(II)_{ox}$ was the dominant reduced Fe pool in the case of hematite (Fig. 1).

At circumneutral pH and above, rates of $Fe(II)_{ox}$ dissolution are significantly reduced, as protonation of the nearest attached oxide or hydroxide ion is required to promote dissolution (Zinder et al., 1986). Thus, in our experiments with lepidocrocite at pH 8.6 and ferrihydrite at pH 8.5 and 9.1, the majority of the reduced Fe remained associated with the oxide surface on the time-scale of these experiments, with only minor proportions of $Fe(II)_{aq}$ and FeS produced (Fig. 1E–G). At these higher pH values, the solubility of FeS is dominated by dissolved sulfide complexes ($Fe(HS)_2$ and FeS^0_{aq} clusters; Rickard, 2006), and speciation calculations in Phreeqc suggest that these make up to ~82 % of total $Fe(II)_{aq}$, due to the persistence of dissolved sulfide. We note that in the majority of experiments, sulfide was still present in solution and hence the reaction was still in progress (with the exception of the experiment with ferrihydrite at pH 4.0; see Table 1).

In order to assess the potential role of differences in mineral reactivity, and to evaluate the reliability of these experiments in terms of their application to assessing associated Fe isotope fractionations, it is instructive to consider both absolute reaction rates and general orders of mineral reactivity relative to previous studies. Poulton (2003) and Poulton et al. (2004) defined the rate equation for sulfide-promoted Fe(III) dissolution of different Fe (oxyhydr)oxide minerals as:

$$R_{Fe} = k_{Fe}(H_2S)^{0.5}_{t=0}\ (Fe^{III})_{t=0} \quad (9)$$

where R_{Fe} represents the initial rate of Fe(III) dissolution (in mol L^{-1} min^{-1}), k_{Fe} is the rate constant (in $mol^{-0.5}$ $L^{0.5}$ min^{-1}), $(H_2S)_{t=0}$ is the initial sulfide concentration (in mol L^{-1}), and $(Fe^{III})_{t=0}$ is the initial concentration of solid phase ferric Fe (in mol L^{-1}). Because some of the Fe(II) released from the mineral surface immediately reacts to form FeS, we calculate the amount of Fe(II) liberated ($Fe(II)_{lib}$) as $Fe(II)_{aq}$ plus Fe present as solid phase FeS. The initial phase of Fe(III) dissolution is linear, allowing initial dissolution rates to be determined via simple linear regression (Fig. 2) (see Poulton, 2003; Poulton et al., 2004). The resulting rate constants demonstrate that reactivity at pH 4 increased in the order hematite ($k_{Fe} = 1.6 \times 10^{-2}$ $mol^{-0.5}$ $L^{0.5}$ min^{-1}) < goethite (k_{Fe}

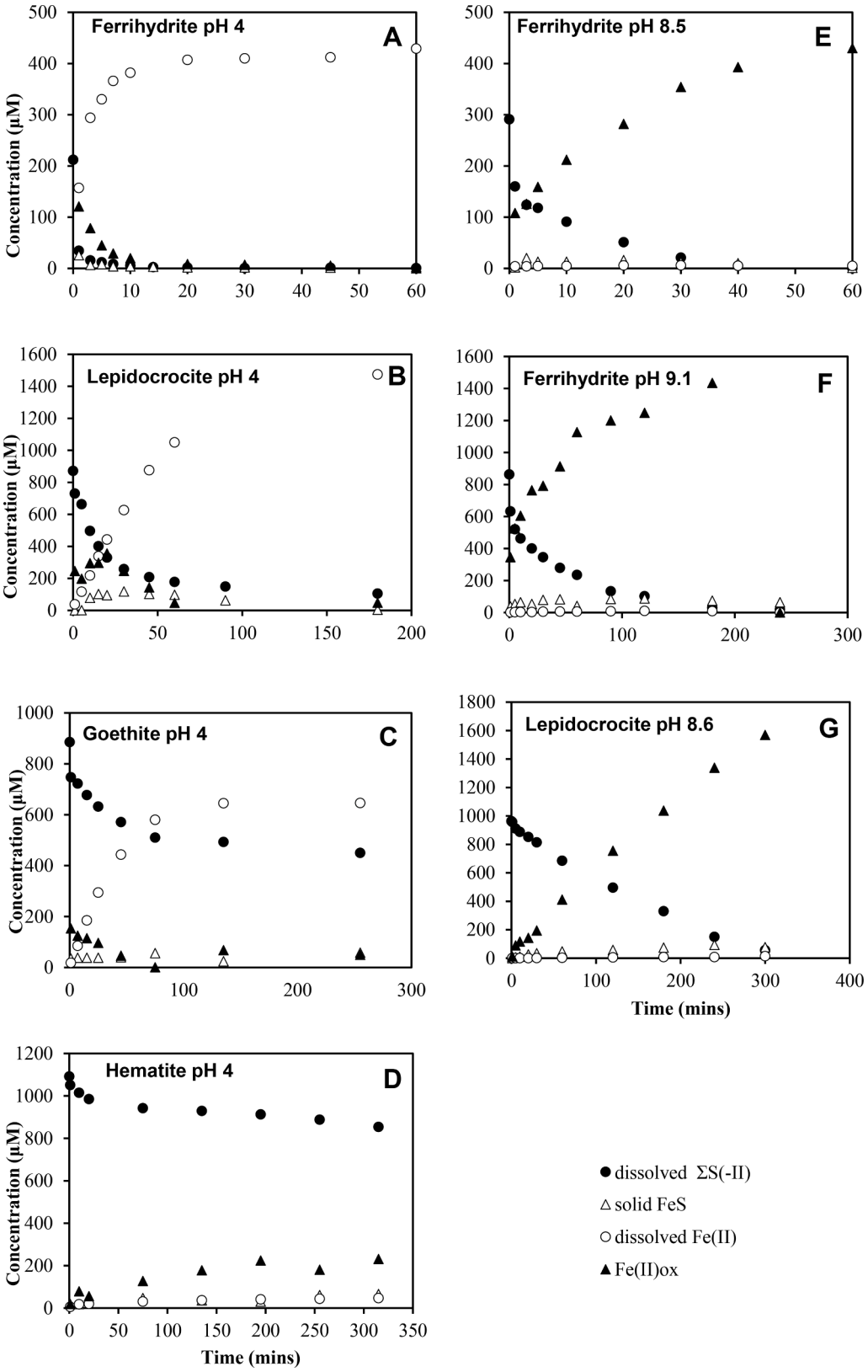

Fig. 1. Chemical speciation data for sulfidation experiments performed at pH 4 (A-D) and pH >8 (E–G). Data for surface-reduced Fe is calculated from the total Fe(II) mass balance (see text for details). Error bars (based on replicate analyses of stock solutions) are within the size of the data symbols.

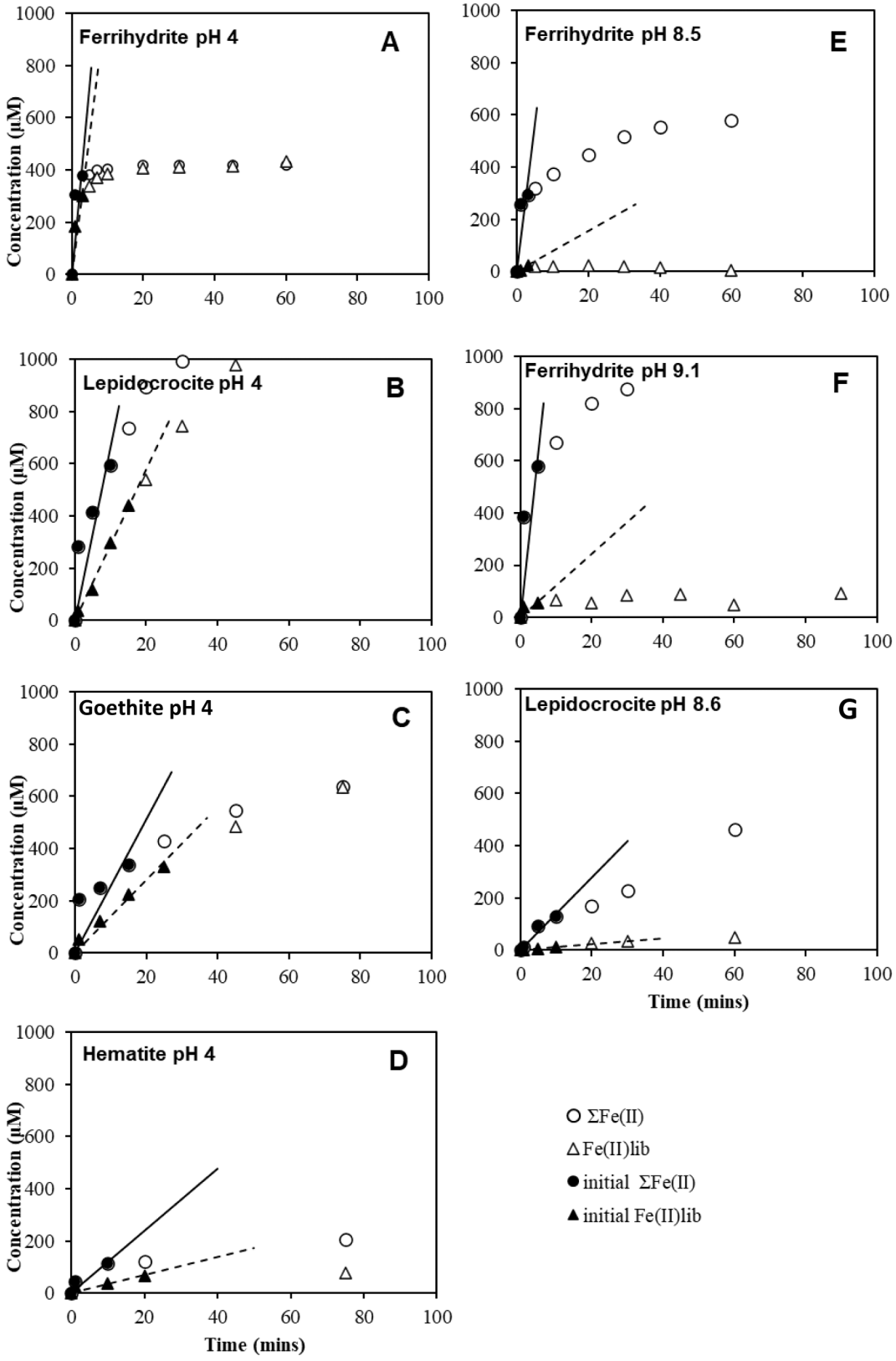

Fig. 2. Temporary variations of total reduced Fe ($\Sigma Fe(II) = Fe^{2+}_{aq} + FeS + Fe(II)_{ox}$) and the amount of reduced Fe liberated into solution ($Fe(II)_{lib} = Fe^{2+}_{aq} + FeS$). Filled symbols indicate the linear phase of the experiment, which were used to calculate reaction rates for the initial stages of the experiments.

$= 8.2 \times 10^{-2}$ mol$^{-0.5}$ L$^{0.5}$ min^{-1}) < lepidocrocite ($k_{Fe} = 35.1 \times 10^{-2}$ mol$^{-0.5}$ L$^{0.5}$ min^{-1}) < ferrihydrite ($k_{Fe} = 63.0 \times 10^{-2}$ mol$^{-0.5}$ L$^{0.5}$ min^{-1}). The increased reactivity of ferrihydrite and lepidocrocite, relative to the more ordered goethite and hematite minerals, is consistent with previous studies at pH 7.5, although overall rates are 1–3 orders of magnitude higher at pH 4 (Poulton et al., 2004). Peiffer and Gade (2007) found that Fe (oxyhydr)oxide reactivity was reversed at low pH, with goethite being more reactive towards dissolved sulfide than ferrihydrite. Our data suggest that the reactivity of goethite approaches that of ferrihydrite at pH 4, but we find no evidence for a reversal in the order of reactivity for the different minerals.

A direct comparison can also be made between previous studies of ferrihydrite dissolution at pH 4 (Poulton, 2003) and our experiment performed under similar conditions. Recasting Eqn. (9) in terms of initial surface area (in m^2 g^{-1}) instead of $(Fe^{3+})_{t=0}$ allows experiments performed with different batches of ferrihydrite to be compared (reactivity depends on relative surface area, rather than the absolute mass of different mineral batches used in the experiments). The similarity in the calculated rate constants ($k_{Fe} = 2.7 \times 10^{-5}$ mol$^{0.5}$ L$^{0.5}$ m^{-2} min^{-1} in the present study, compared to $k_{Fe} = 2.6 \times 10^{-5}$ mol$^{0.5}$ L$^{0.5}$ m^{-2} min^{-1} in Poulton, 2003) provides support for the robust nature of our experimental procedure.

4.2. Fe Isotope compositions

Non-reductive dissolution experiments with 6 N HCl, which were conducted to check for isotopic homogeneity of the starting Fe-oxide mineral, show contrasting results for goethite and hematite (Table 3). With the exception of the first sample, the initial dissolution of the surface of goethite produced dissolved Fe that was isotopically heavier than the bulk mineral, suggesting that the synthetic mineral was likely zoned (with a ^{56}Fe-enriched rim), since non-reductive dissolution of Fe (oxyhydr)oxides does not tend to impart an isotopic fractionation (Wiederhold et al., 2006), particularly at high HCl concentration (6 N). Isotopic zonation may occur as a result of a kinetic effect during goethite precipitation at medium temperature (see section 3.1), which may not favour extensive isotope exchange. Although we were not able to perform this check on lepidocrocite, it is plausible that this mineral may also have an isotopically enriched rim, as its synthesis involves $Fe(II)_{aq}$ oxidation at room temperature. By contrast, during hematite dissolution, δ^{56}Fe compositions of dissolved Fe were on average somewhat lighter than the bulk mineral during the initial dissolution stages, but the majority of these analyses were within error of the hematite bulk sample. The absence of isotopic zonation likely reflects insignificant kinetic effects during hematite synthesis at higher temperature (see section 3.1), which may promote isotope exchange and homogenization during precipitation.

Table 3
Isotope composition of dissolved Fe during incremental non-reductive dissolution of Fe-oxide mineral with 6 N HCl. All isotope analyses are normalised to the bulk Fe isotope composition of each starting mineral; n = number of replicate analyses.

	Fe dissolved (%)	δ^{56}Fe (‰)	δ^{57}Fe (‰)	n
Goethite	0.7	−0.12 ± 0.11	−0.10 ± 0.20	4
	0.9	0.09 ± 0.02	0.20 ± 0.12	4
	2.3	0.28 ± 0.01	0.38 ± 0.08	2
	3.4	0.37 ± 0.04	0.59 ± 0.06	3
	4.4	0.26 ± 0.03	0.48 ± 0.15	3
	6.3	0.34 ± 0.15	0.53 ± 0.30	4
	8.6	0.27 ± 0.09	0.45 ± 0.09	2
	9.8	0.27 ± 0.21	0.46 ± 0.30	4
	12.1	0.45 ± 0.12	0.70 ± 0.10	4
	100.0	−0.02 ± 0.09	−0.02 ± 0.09	4
Hematite	1.4	−0.05 ± 0.07	−0.07 ± 0.17	4
	2.9	−0.08 ± 0.16	−0.09 ± 0.33	4
	9.8	−0.04 ± 0.15	−0.09 ± 0.26	4
	12.6	−0.11 ± 0.17	−0.11 ± 0.13	4
	14.9	−0.15 ± 0.15	−0.22 ± 0.24	4
	20.0	−0.08 ± 0.00	−0.19 ± 0.17	2
	23.0	−0.07 ± 0.17	−0.13 ± 0.28	4
	27.7	−0.17 ± 0.03	−0.33 ± 0.05	2
	28.0	−0.03 ± 0.08	−0.06 ± 0.08	4
	100.0	0.00 ± 0.16	−0.02 ± 0.19	4

Iron isotope compositions were determined for $Fe(II)_{aq}$, $Fe(II)_{solid}$ (defined as $Fe(II)_{ox}$ + FeS), and unreacted Fe(III) ($Fe(III)_{unreac}$; Tables 1 and 3). The isotope compositions for total Fe ($\delta^{56}Fe_T$; Tables 1 and 2) were calculated on ~20 % of the samples, as the weighted sums of the three measured isotope pools (Eqn. (10)):

$$\delta^{56}Fe_T = \left(\frac{[Fe(II)_{aq}]}{[Fe_T]} \times \delta^{56}Fe_{Fe(II)aq}\right) + \left(\frac{[Fe(II)_{solid}]}{[Fe_T]} \times \delta^{56}Fe_{Fe(II)solid}\right) + \left(\frac{[Fe(III)_{unreac}]}{[Fe_T]} \times \delta^{56}Fe_{Fe(III)unreac}\right) \quad (10)$$

Our data give an average isotopic mass balance close to zero (0.02 ± 0.03 ‰, 2σ, n = 10), providing strong support for the validity of our Fe (II) pool calculations and the robustness of our experimental approach.

In the majority of experiments conducted at pH 4, the $Fe(II)_{aq}$ pool was isotopically lighter than the $Fe(II)_{solid}$ pool, with the exception of the first ferrihydrite sample and the reaction with lepidocrocite, where Fe (II) products are hardly distinguishable (Fig. 3). The dissolved phase was also isotopically lighter than the starting mineral (i.e., $\delta^{56}Fe < 0$) for ferrihydrite and hematite, with compositions down to −0.23 ± 0.11 ‰ and −0.51 ± 0.07 ‰, respectively. We note that for these minerals, however, solid Fe(II) products were dominantly heavier than the starting material, with compositions up to 0.31 ± 0.04 ‰ and 0.36 ± 0.10 ‰ for ferrihydrite and hematite, respectively. By contrast, for lepidocrocite and goethite, almost all Fe products were isotopically heavier than the starting mineral, with compositions up to 0.31 ± 0.04 ‰ for lepidocrocite, and 0.58 ± 0.02 ‰ for goethite.

For experiments conducted at alkaline pH, Fe(II) products were isotopically lighter than the starting material for ferrihydrite, while in the case of lepidocrocite, Fe(II) products were heavier, with the $Fe(II)_{aq}$ pool isotopically lighter than the $Fe(II)_{solid}$ pool (Fig. 3). We note that the two Fe(II) pools had a similar isotope composition for the experiment with ferrihydrite at pH 8.5, clustering around ~−0.6 ‰, while the $Fe(II)_{aq}$ pool is on average ~0.4 ‰ lighter than the solid Fe(II) product for the experiment at pH 9.1.

5. Discussion

5.1. Mechanistic controls on Fe isotope fractionation

5.1.1. Secondary adsorption effects

In order to evaluate controls on isotopic fractionation during both the reductive and dissolution phases of this reaction, it is important to consider a potential secondary overprint which may result from $Fe(II)_{aq}$ adsorption at the oxide surface. This process has been suggested to produce a significant isotope fractionation (≥2.5 ‰) between aqueous Fe(II) and Fe-oxide minerals, attributed to preferential adsorption of heavier isotopes onto the oxide surface (Icopini et al., 2004; Teutsch et al., 2005). Subsequent experiments investigating the surface interaction between aqueous Fe(II) and a range of minerals (ferrihydrite, hematite and goethite) have confirmed the preferential sorption of heavier Fe(II), albeit with a smaller isotope fractionation between $Fe(II)_{aq}$ and sorbed Fe(II), ranging from ~0.5 to 1.3 ‰ (Wu et al., 2009, 2011; Mikutta et al., 2009; Beard et al., 2010).

At first glance, our experimental results at low pH may reflect the preferential adsorption of heavy isotopes onto the mineral surface, leaving an isotopically depleted residual $Fe(II)_{aq}$ pool (Fig. 3). However, we argue that at pH 4, adsorption of $Fe^{2+}_{(aq)}$ is negligible on the positively charged surfaces of Fe (oxyhydr)oxide and FeS (Silvester et al., 2005;

Wolthers et al., 2005), and is thus unlikely to exert any influence on our experiments at low pH (see also Wiederhold et al., 2006). By contrast, at higher pH, the increase in positively charged sites at mineral surfaces may enhance $Fe(II)_{aq}$ re-adsorption effects. Poulton (2003), however, suggested that adsorption of $Fe(II)_{aq}$ would not be a significant process providing sulfide remains in solution (which was the case for our experiments at alkaline pH, since isotopic measurements were only made for samples taken while sulfide was still present in solution; Table 2). Under these conditions, FeS forms almost instantaneously (Rickard, 1995) and its limited solubility is dominated by the neutrally charged dissolved $FeS^0_{(aq)}$ species (Rickard, 2006). This is further confirmed by Fe $(II)_{aq}$ speciation calculations, which show a substantially decreased proportion of $Fe^{2+}_{(aq)}$, in favour of sulfide complexes. Furthermore, direct measurements of adsorbed Fe(II) during sulfidation reactions with ferrihydrite at alkaline pH (using $CaCl_2$ as an extractant for adsorbed Fe (II)), showed that at the end of experiments when dissolved sulfide was completely reacted from solution, adsorbed Fe(II) accounted for <2 % of the total Fe(II) pool (Poulton, 2003). In fact, after all dissolved sulfide has reacted from solution, Fe(II) associated with the oxide surface continues to decrease (due to the slow dissolution of $Fe(II)_{ox}$), rather than increase (due to potential re-adsorption of $Fe(II)_{aq}$). Thus, whilst we cannot entirely rule out adsorption effects at higher pH, it is unlikely that $Fe(II)_{aq}$ that has truly escaped the influence of the oxide surface outer-sphere could extensively re-adsorb onto Fe-oxides and FeS surfaces. In fact, for all higher-pH experiments, the lack of a large fractionation between $Fe(II)_{aq}$ and solid Fe(II) (Fig. 3) further argues against the typical Fe isotope fractionations expected in association with adsorption effects.

However, as discussed below, even minor re-adsorption at higher pH may permit electron transfer to the mineral surface and subsequently to the bulk mineral, with potential isotope fractionations (e.g., Crosby et al., 2005, 2007; Handler et al., 2009). Hence, while we propose that Fe isotope fractionations commonly associated with re-adsorption are likely to be muted in our experiments, the process may contribute to fractionations associated with electron transfer and the general mineral reduction step.

5.1.2. Reduction-dominated Fe isotope fractionation

The three major ferrous Fe pools that are generated during reductive dissolution of Fe (oxyhydr)oxides by sulfide are $Fe(II)_{aq}$, Fe(II) associated with the oxide surface (i.e., $Fe(II)_{ox}$ from Eqs. (2)–(4)), and $Fe(II)_{aq}$ that has reacted with sulfide to form FeS. The isotope composition of the combined Fe(II) pools ($\delta^{56}Fe_{\Sigma Fe(II)}$) can be calculated through simple isotope mass balance, as $Fe(II)_{ox}$ and FeS were measured as a single

Table 4
Calculated isotope fractionations for the reductive ($\Delta^{56}\Sigma Fe_{Fe(II)}$) and dissolution ($\Delta^{56}Fe_{Fe(II)lib-Fe(II)ox}$) steps of the reaction mechanism, and $Fe^{2+}_{(aq)}$ isotope compositions corrected for the influence of FeS precipitation ($\delta^{56}Fe_{Fe(II)lib}$). $\Sigma Fe(II)/Fe_T$ refers to the proportion (%) of the bulk mineral that has been reduced. Apart from $\Delta^{56}\Sigma Fe_{Fe(II)}$, errors are 2σ and were derived through standard error propagation.

Experiment	Time (mins)	$\Sigma Fe(II)/Fe_T$ (%)	$Fe_{\Sigma Fe(II)}$ (μM)	$Fe_{Fe(II)lib}$ (μM)	$\delta^{56}Fe_{\Sigma Fe(II)}$ (‰)	$\delta^{56}Fe_{Fe(II)lib}$ (‰)	$\delta^{56}Fe_{Fe(II)ox}$ (‰)	$\Delta^{56}Fe_{\Sigma Fe(II)\ -\ Fe\text{-}oxide}$ (‰)	$\Delta^{56}Fe_{Fe(II)lib\ -\ Fe(II)ox}$ (‰)
Ferrihydrite	1	2.6	304	183	−0.18 ± 0.08	−0.25 ± 0.31	−0.06 ± 0.30	−0.18 ± 0.08	−0.19 ± 0.43
1.0 g/L; pH 4	3	3.2	379	301	−0.19 ± 0.11	−0.24 ± 0.32	0.01 ± 0.30	−0.19 ± 0.11	−0.25 ± 0.44
	5	3.2	383	338	−0.13 ± 0.23	−0.19 ± 0.37	0.36 ± 0.32	−0.13 ± 0.23	−0.55 ± 0.48
	7	3.4	399	370	−0.13 ± 0.12	−0.17 ± 0.32	0.35 ± 0.30	−0.13 ± 0.12	−0.52 ± 0.44
	10	3.4	406	386	−0.08 ± 0.09	−0.11 ± 0.31	0.54 ± 0.30	−0.08 ± 0.09	−0.65 ± 0.43
	20	3.5	417	409	−0.12 ± 0.17	−0.13 ± 0.32	0.52 ± 0.33	−0.12 ± 0.17	−0.65 ± 0.46
	30	3.5	419	412	−0.15 ± 0.15	−0.16 ± 0.31	0.54 ± 0.33	−0.15 ± 0.15	−0.70 ± 0.45
	45	3.5	419	413	−0.09 ± 0.08	−0.10 ± 0.31	0.60 ± 0.30	−0.09 ± 0.08	−0.70 ± 0.43
	60	3.6	432	432	−0.12 ± 0.19	−0.12 ± 0.34		−0.12 ± 0.19	
Lepidocrocite	10	21.1	592	297	0.18 ± 0.05	−0.05 ± 0.30	0.42 ± 0.30	0.18 ± 0.05	−0.48 ± 0.43
0.25 g/L; pH 4	20	31.8	894	538	0.10 ± 0.17	0.00 ± 0.31	0.27 ± 0.34	0.10 ± 0.17	−0.27 ± 0.46
	45	36.4	1122	979	0.06 ± 0.19	−0.03 ± 0.31	0.66 ± 0.34	0.06 ± 0.19	−0.69 ± 0.46
Goethite	1	3.7	206	53	0.14 ± 0.11	−0.58 ± 0.31	0.38 ± 0.32	0.14 ± 0.11	−0.96 ± 0.44
0.5 g/L; pH 4	15	8.5	476	190	0.30 ± 0.19	0.12 ± 0.32	0.42 ± 0.34	0.30 ± 0.19	−0.84 ± 0.46
	45	9.4	529	483	0.33 ± 0.22	0.19 ± 0.34	1.73 ± 0.34	0.33 ± 0.22	−1.54 ± 0.48
	135	13.1	737	669	0.29 ± 0.10	0.21 ± 0.32	1.09 ± 0.30	0.29 ± 0.10	−0.88 ± 0.44
	255	13.4	754	704	0.23 ± 0.18	0.13 ± 0.30	1.68 ± 0.35	0.23 ± 0.18	−1.56 ± 0.46
Hematite	1	0.7	44	25	0.19 ± 0.11	−0.72 ± 0.31	1.40 ± 0.32	0.19 ± 0.11	−2.12 ± 0.44
0.5 g/L; pH 4	20	2.0	122	66	0.09 ± 0.12	−0.75 ± 0.31	1.07 ± 0.32	0.09 ± 0.12	−1.82 ± 0.44
	75	3.3	206	78	0.17 ± 0.14	−0.71 ± 0.32	0.71 ± 0.32	0.17 ± 0.14	−1.42 ± 0.45
	195	4.7	296	72	0.25 ± 0.24	−0.65 ± 0.37	0.53 ± 0.32	0.25 ± 0.24	−1.18 ± 0.49
Ferrihydrite	1	1.9	114	6	−0.63 ± 0.14	−0.65 ± 0.32	−0.62 ± 0.32	−0.63 ± 0.14	−0.02 ± 0.45
0.5 g/L; pH 8.5	3	2.5	150	24	−0.52 ± 0.10	−0.81 ± 0.32	−0.47 ± 0.30	−0.52 ± 0.10	−0.34 ± 0.44
	5	3.0	176	17	−0.53 ± 0.27	−0.81 ± 0.40	−0.50 ± 0.30	−0.53 ± 0.27	−0.30 ± 0.50
	20	5.1	304	22	−0.59 ± 0.22	−0.78 ± 0.31	−0.58 ± 0.36	−0.59 ± 0.22	−0.20 ± 0.48
	30	6.3	372	18	−0.63 ± 0.11	−0.80 ± 0.31	−0.62 ± 0.31	−0.63 ± 0.11	−0.17 ± 0.44
Ferrihydrite	1	4.7	386	40	−0.43 ± 0.21	−0.84 ± 0.32	−0.38 ± 0.35	−0.43 ± 0.21	−0.46 ± 0.47
0.7 g/L; pH 9.1	10	8.1	672	67	−0.36 ± 0.25	−0.84 ± 0.31	−0.31 ± 0.38	−0.36 ± 0.25	−0.54 ± 0.49
	60	14.2	1174	47	−0.23 ± 0.26	−0.82 ± 0.31	−0.20 ± 0.39	−0.23 ± 0.26	−0.61 ± 0.50
	120	16.2	1346	98	−0.15 ± 0.08	−0.83 ± 0.31	−0.10 ± 0.30	−0.15 ± 0.08	−0.73 ± 0.43
Lepidocrocite	30	6.8	230	36	0.16 ± 0.05	−0.81 ± 0.30	0.33 ± 0.30	0.16 ± 0.05	−1.14 ± 0.43
0.3 g/L; pH 8.6	60	13.7	462	50	0.21 ± 0.10	−0.80 ± 0.30	0.33 ± 0.31	0.21 ± 0.10	−1.13 ± 0.44
	180	33.2	1118	81	0.17 ± 0.06	−0.77 ± 0.30	0.24 ± 0.31	0.17 ± 0.06	−1.01 ± 0.43
	300	49.2	1660	91	0.20 ± 0.07	−0.71 ± 0.30	0.25 ± 0.31	0.20 ± 0.07	−0.96 ± 0.43

isotopic pool (i.e., $Fe(II)_{solid}$ in our experiments):

$$\delta^{56}Fe_{\Sigma Fe(II)} = \left(\frac{[Fe(II)_{aq}]}{[\Sigma Fe(II)]} \times \delta^{56}Fe_{Fe(II)aq}\right) + \left(\frac{[Fe(II)_{solid}]}{[\Sigma Fe(II)]} \times \delta^{56}Fe_{Fe(II)solid}\right) \quad (11)$$

Because our measured isotope compositions are normalized to the isotope composition of the starting material, $\delta^{56}Fe_{\Sigma Fe(II)}$ is equivalent to the isotope fractionation attributable to the overall reduction-dominated step during sulfidation (Table 4 and Fig. 4).

We start with our alkaline-pH experiments, which were designed to hamper extensive dissolution to allow focus on Fe isotope fractionations dominantly associated with the reduction process. Because the production of dissolved $Fe(II)_{aq}$ is significantly diminished at higher pH (Fig. 1), the difference between $\delta^{56}Fe_{Fe(II)solid}$ and $\delta^{56}Fe_{\Sigma Fe(II)}$ is only minor (Figs. 3 and 4). We note that for the ferrihydrite experiments, which correspond to the lowest extent of reduction (with low $Fe(II)/Fe_T$; Tables 2 and 4) but also to the fastest reduction rates (Fig. 2; Table 5), both the $Fe(II)_{solid}$ and $Fe(II)_{aq}$ pools are enriched in the light isotopes, with $\delta^{56}Fe_{\Sigma Fe(II)}$ down to ~ -0.6 ‰. Hence, the reductive step of the reaction is characterized by a kinetic incorporation of light isotopes in the reduced ΣFe(II) pool (Fig. 4). We note that with higher extents of reduction (i.e., for the ferrihydrite experiment at pH 9.1), the isotopic composition of the $Fe(II)_{solid}$ pool becomes less negative.

At a slower mineral reduction rate, as is the case for the lepidocrocite experiment, the isotopic composition of the $Fe(II)_{solid}$ pool becomes slightly positive, presumably reflecting a higher extent of isotope exchange at slower reaction rates, as opposed to rapid reaction rates which favour the expression of kinetic effects. We mentioned above that synthetic lepidocrocite may exhibit a ^{56}Fe-enriched rim, which could lead to apparent high δ^{56}Fe compositions in the ΣFe(II) pool. However, the large proportion of $Fe(II)_{ox}$ in the lepidocrocite experiments (Table 1) implies that the reduction of any potential ^{56}Fe-enriched-rim should have been exhausted, and we conclude that the persisting positive $\delta^{56}Fe_{Fe(II)ox}$ values do not reflect a zonation overprint. Handler et al. (2009) showed that for well-ordered oxyhydroxides, isotope exchange between the bulk mineral and its aqueous media readily occurs, due to electron-transfer towards the bulk mineral structure. This mechanism was also proposed by Crosby et al. (2005) during DIR, whereby isotope fractionations are suggested to be generated by atom and electron exchange between $Fe^{2+}_{(aq)}$ and a reactive layer of Fe(III) at the oxide surface. This contrasts greatly with the less-ordered ferrihydrite, which shows limited isotope exchange with the media (Poulson et al., 2005), presumably due to its nanocrystalline size (Michel et al., 2007; but see also Guilbaud et al., 2010; Chanda et al., 2021 for discussions on isotope exchange within nanoparticles). Electron-transfer towards the bulk mineral structure, which may result in expansive reduction beyond the mineral surface, is reflected by the formation of magnetite and FeS upon sulfidation of FeOOH (Hellige et al., 2012). Our results for the lepidocrocite experiments support this process, with a large extent of mineral reduction and the formation of a slightly ^{56}Fe-enriched $Fe(II)_{ox}$ pool (Fig. 3G). This is entirely consistent with early-stage isotope exchange between $Fe(II)_{aq}$ and magnetite (e.g., Frierdich et al., 2014) but also with FeS at alkaline pH (Wu et al., 2012a). Therefore, we conclude that under alkaline pH, the reduction step is accompanied by a significant kinetic Fe isotope fractionation, modulated by the extent of isotope exchange, which depends upon Fe (oxyhydr)oxide structure and reactivity, and therefore on the rates of mineral reduction.

Under acidic conditions (pH 4), we note that the speciation results for hematite, which shows the slowest reduction rates, are also characterized by limited dissolution and rather extensive formation of $Fe(II)_{ox}$ (Fig. 1D). In this sense, results may be interpreted in a similar manner to the alkaline lepidocrocite experiments, whereby a lower mineral reactivity results in the formation of a slightly heavier $Fe(II)_{ox}$ pool, relative to the bulk mineral, due to a higher potential for isotopes to exchange. A major difference between the hematite (pH 4) and the lepidocrocite (pH 8.6) experiments relates to the Fe isotope composition of $Fe(II)_{aq}$, with δ^{56}Fe down to -0.51 ± 0.07 ‰ in the case of the hematite experiment, while the lepidocrocite (pH 8.6) experiment systematically produced heavier (δ^{56}Fe >0 ‰) $Fe(II)_{aq}$ (Fig. 3). These different $Fe(II)_{aq}$ compositions likely reflect formation of a larger proportion of isotopically heavier $Fe(HS)_2$ species in the lepidocrocite experiments at higher pH (Table 2, Wu et al., 2012a).

For all other minerals at pH 4, we observe a substantially higher release of dissolved $Fe(II)_{aq}$, which may overprint the Fe isotope signature from the reduction step. However, Eqn. (11) and the resulting $\Delta^{56}Fe_{\Sigma Fe(II)-Fe\text{-}oxide}$ (which is the difference between $\delta^{56}Fe_{\Sigma Fe(II)}$ and $\delta^{56}Fe_{Fe\text{-}oxide}$) accounts for all Fe(II) species produced, regardless of the dissolution process. For ferrihydrite, the lighter isotope accumulates preferentially in the $Fe(II)_{aq}$ pool, as for the higher pH experiments. This leaves $Fe(II)_{ox}$, which dominates the $Fe(II)_{solid}$ pool at this pH, with heavier isotopic signatures (Fig. 3A). The total ΣFe(II) products are isotopically lighter than the Fe(III) mineral (Fig. 4A). For goethite and lepidocrocite, however, the reductive step results in $Fe(II)_{aq}$ and ΣFe(II) that are isotopically heavier than the bulk mineral (Fig. 4B and C). In the case of goethite, the ΣFe(II) produced in the reductive step $\Delta^{56}Fe_{\Sigma Fe(II)-Fe\text{-}oxide} = 0.33 \pm 0.20$ ‰ when 9.4 % of the mineral is reduced; Table 4), is similar to that released at the same stage of the reaction by non-reductive dissolution with 6N HCl (δ^{56}Fe = 0.27 ± 0.21 ‰ at 9.8 % dissolution; Table 3), clearly suggesting that this is an artefact relating to the presence of an isotopically-heavy rim on the mineral. For this reason, results for the goethite experiments are excluded from further discussion. By contrast, as mentioned above in the case of lepidocrocite, a potential isotopically heavy rim would have been consumed by the large extent of reduction (Table 4), and therefore the ^{56}Fe enrichments observed in ΣFe(II) (Figs. 3 and 4) cannot be attributed to isotope zonation. Instead, we propose that, as for ferrihydrite, solid reduction products ($Fe(II)_{solid}$) are slightly enriched in ^{56}Fe. By comparison with the ferrihydrite experiment, there is a larger proportion of FeS as a reduction product during lepidocrocite sulfidation, which has also been demonstrated by TEM and spectroscopic techniques (Hellige et al., 2012; Wan et al., 2014). The persistence of FeS may explain the relatively lighter compositions for $Fe(II)_{solid}$ relative to $Fe^{2+}_{(aq)}$ at low pH, albeit with significant exchange between the solid pool and the large, dissolved pool (Butler et al., 2005; Guilbaud et al., 2010; Wu et al., 2012a).

Together, our results at low and high pH suggest that the Fe isotope composition of dissolved and solid reduced products depends on the speciation of dissolved $Fe(II)_{aq}$ (triggered by pH), the structure and reactivity of the starting material, the extent of mineral reduction, and the reduction rates themselves. The full range of potential Fe(II) products is summarised by Fig. 5. We next explore controls on the magnitude of the reduction step (i.e., $\Delta^{56}Fe_{\Sigma Fe(II)-Fe\text{-}oxide}$) by considering the experiments performed with ferrihydrite under different conditions. For the ferrihydrite experiments conducted at pH 4.0 and 8.5, there is no consistent trend in the magnitude of $\Delta^{56}Fe_{\Sigma Fe(II)-Fe\text{-}oxide}$ fractionations as the reaction progresses (Table 4, Fig. 4A, E and F). Hence it is not simply the extent of reduction and dissolution of surface layers that controls the magnitude of the reductive step isotope fractionations. If this were the case (i.e., if new surface sites were not generated rapidly enough due to the slow release of $Fe(II)_{ox}$ to solution), then $\Delta^{56}Fe_{\Sigma Fe(II)-Fe\text{-}oxide}$ fractionations would decrease rapidly as the reaction progresses and approach zero at an early stage of the experiment. This is, in fact, observed for the experiment at pH 9.1 (Fig. 4F), where a significant proportion of the mineral is reduced with only minor release of $Fe(II)_{aq}$ to solution (Table 1). In this experiment, it is clear that the lighter isotope is initially preferentially reduced and released to solution (similar to the other two ferrihydrite experiments, Fig. 6), but due to the slow release of $Fe(II)_{ox}$ at high pH, available surface sites become increasingly limited and thus $\Delta^{56}Fe_{\Sigma Fe(II)-Fe\text{-}oxide}$ fractionations become progressively smaller with time.

To evaluate the magnitude of isotope fractionation during the early

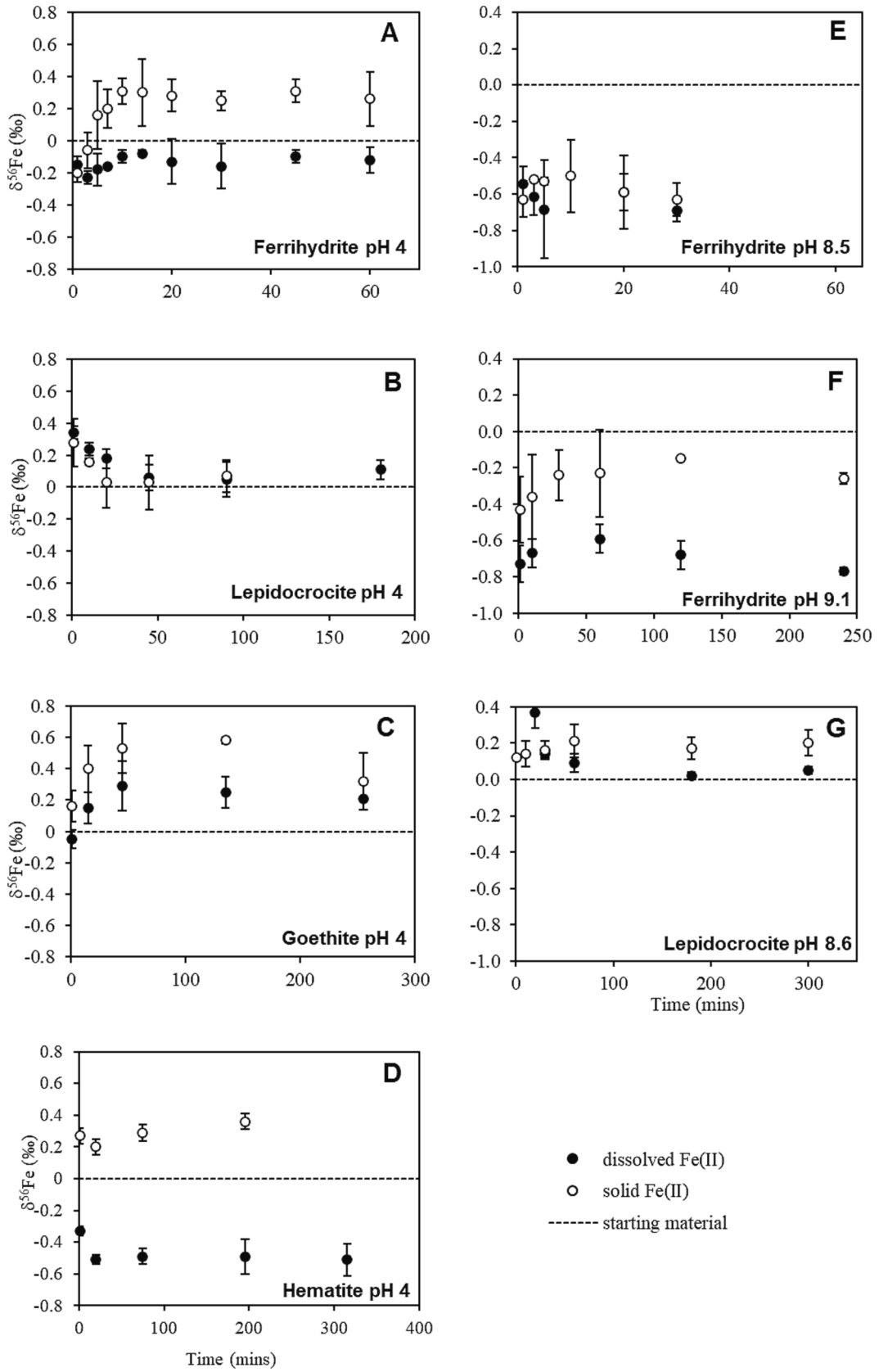

Fig. 3. Measured iron isotope compositions ($\delta^{56}Fe$) of dissolved Fe^{2+} (black circles), and solid Fe(II), defined as $Fe(II)_{ox}$ + FeS (open circles), for experiments performed at pH 4 (A-D) and pH >8 (E-G). The dashed line at 0 ‰ marks the isotope composition of the starting material. Error bars are 2σ.

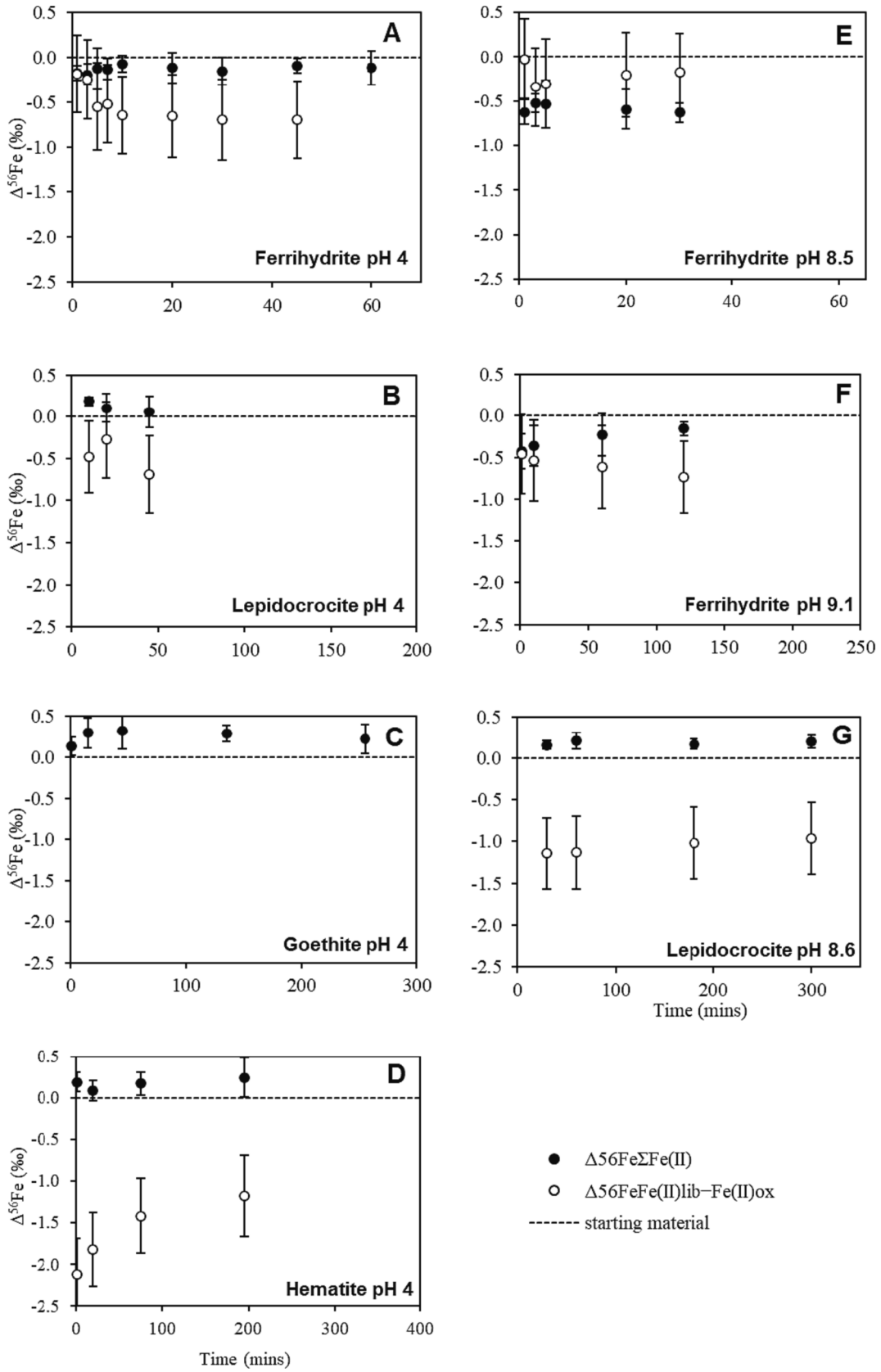

Fig. 4. Calculated isotope fractionations for the reduction step ($\Delta^{56}Fe_{\Sigma Fe(II)-Fe\text{-}oxide}$) and dissolution step ($\Delta^{56}Fe_{Fe(II)lib-Fe(II)ox}$) during the reactions at pH 4 (A-D) and pH >8 (E-G). Error bars are 2σ. Note that $\Delta^{56}Fe_{Fe(II)lib-Fe(II)ox}$ values for the goethite experiments are not plotted or discussed, due to the presence of an isotopic zonation between the rim and mineral core.

Table 5
Calculated initial reaction rates for Fe(III) reduction and Fe(II) dissolution, and their associated average isotope fractionations ($\Delta^{56}\Sigma Fe_{Fe(II)}$ and $\Delta^{56}Fe_{Fe(II)lib-Fe(II)ox}$, respectively). Rates were calculated from linear regression (see Fig. 2). Errors are 2σ and were derived through standard error propagation; n.c. stands for 'not calculated', because of isotopic heterogeneity of the initial Fe-oxide or because initial isotope data are lacking.

Experiment	Fe(III) reduction rate		$\Delta^{56}Fe_{\Sigma Fe(II)}$	Fe(II) dissolution rate		$\Delta^{56}Fe_{Fe(II)lib-Fe(II)ox}$
	(μM/min)	R^2	(‰)	(μM/min)	R^2	(‰)
Ferrihydrite pH 4	144	0.65	−0.18 ± 0.10	109	0.86	−0.22 ± 0.43
Lepidocrocite pH 4	62	0.72	−0.18 ± 0.05	29	0.99	−0.48 ± 0.43
Goethite pH 4	33	0.73	n.c.	14	0.96	−1.11 ± 0.46
Hematite pH 4	12	0.85	−0.19 ± 0.11	3.4	0.79	−1.97 ± 0.44
Ferrihydrite pH 8.5	56	0.70	−0.56 ± 0.16	7.8	0.99	−0.22 ± 0.46
Ferrihydrite pH 9.1	126	0.60	−043 ± 0.19	12	0.52	−0.50 ± 0.48
Lepidocrocite pH 8.6	14	0.94	n.c.	1.1	0.99	−1.14 ± 0.43

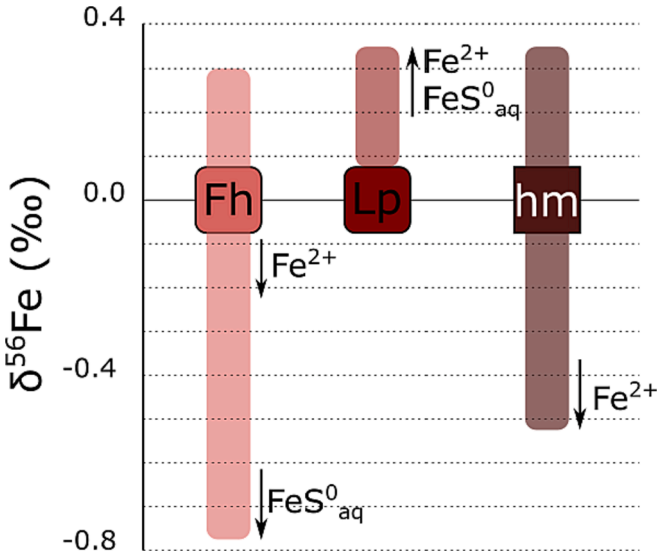

Fig. 5. Summary cartoon of the potential range of all Fe(II) products during ferrihydrite (Fh), lepidocrocite (Lp) and hematite (hm) reduction by sulfide, including both solids and dissolved species at any pH. Squares represent the starting ferric minerals, with Fe isotope compositions of 0 ‰. Shading represents the entire potential range of Fe(II) products. The arrows depict the range of compositions of the dissolved species only (Fe^{2+}_{aq} at low pH and $Fe(HS)_2$ at higher pH).

stage of the experiments, before surface sites become limiting, we compare the average initial $\Delta^{56}Fe_{\Sigma Fe(II)-Fe\text{-}oxide}$ fractionations for ferrihydrite as a function of the initial reduction rate (Fig. 6A). The observed relationships suggest that for one particular mineral structure (e.g., ferrihydrite), it is the *rate* at which the oxide surface is reduced that initially controls the extent of fractionation during the reductive step, with slower rates favouring increased fractionations. The magnitude of reductive-step fractionations is thus a function of the parameters that control reaction rates, including mineral surface area and concentration, sulfide concentration, and pH (Pyzik and Sommer, 1981; Dos Santos and Stumm, 1992; Peiffer et al., 1992; Yao and Millero, 1996; Poulton, 2003; Poulton et al., 2004).

5.1.3. Dissolution-dominated Fe isotope fractionation

Following electron transfer, the second mechanistic part of the sulfidation reaction that may cause Fe isotope fractionation is the dissolution step (Eq. (4)). This fractionation can be calculated from isotope mass balance between the total reduced Fe (ΣFe(II)) and the dissolved Fe $(II)_{aq}$ pools. A complication, however, is that some of the $Fe(II)_{aq}$ released from the mineral surface in our experiments immediately reacts with free sulfide to form FeS. Although our experiments were conducted with the aim of minimizing formation of FeS, this phase was present in all experiments, and in some cases represented a significant proportion of the total Fe(II) pool (Tables 1 and 2). Formation of FeS from $Fe^{2+}_{(aq)}$ (Eqn. (6) is associated with a significant isotope fractionation, and at pH 4, freshly precipitated FeS is 0.85 ± 0.30 ‰ lighter than the co-existing $Fe^{2+}_{(aq)}$ from which it formed (Butler et al., 2005). At pH 4, rapid isotopic exchange between FeS and $Fe^{2+}_{(aq)}$ results in an isotopic steady state, where FeS nanoparticles are 0.27 ± 0.11 ‰ lighter than $Fe^{2+}_{(aq)}$ (Guilbaud et al., 2010). At neutral to alkaline pH, however, FeS may reach isotopic equilibrium with $Fe(II)_{aq}$ species (presumably FeS^0_{aq} and $Fe(HS)_2$), whereby FeS particles are enriched in the heavier isotopes by 0.32 ± 0.29 ‰ (Wu et al., 2012a).

In order to take into account secondary fractionations associated with FeS formation, we estimate the isotopic composition of the Fe(II) released to solution ($\delta^{56}Fe_{Fe(II)lib}$) by assuming an isotopic composition of −0.85 ‰ for freshly precipitated FeS (Butler et al., 2005), according to the isotope mass balance:

$$\delta^{56}Fe_{Fe(II)lib} = \left(\frac{[FeS]}{[Fe(II)_{lib}]} \times \delta^{56}Fe_{FeS}\right) + \left(\frac{[Fe(II)_{aq}]}{[Fe(II)_{lib}]} \times \delta^{56}Fe_{Fe(II)aq}\right) \quad (12)$$

Further, we calculate the isotope composition of the reduced Fe(II) pool at the oxide surface:

$$\delta^{56}Fe_{Fe(II)ox} = \left(\frac{[Fe(II)_{solid}]}{[Fe(II)_{ox}]} \times \delta^{56}Fe_{Fe(II)solid}\right) - \left(\frac{[FeS]}{[Fe(II)_{ox}]} \times \delta^{56}Fe_{FeS}\right) \quad (13)$$

We note that using an isotope composition of −0.85 ‰ for freshly precipitated FeS is conservative, as 1) most of the isotopic exchange following FeS precipitation occurs within the first 4 h of ageing, resulting in a smaller isotope fractionation between $Fe(II)_{aq}$ and FeS (Guilbaud et al., 2010), and 2) the FeS/$Fe(II)_{aq}$ ratios in our experiments are far larger than those used in Butler et al. (2005), further resulting in a lesser expression of the kinetic Fe isotope fractionation between $Fe(II)_{aq}$ and FeS. Therefore, our $\delta^{56}Fe_{Fe(II)lib}$ calculations represent a lower limit of the range of expected compositions. In general, due to the low (i.e., <100 μM FeS) concentrations of FeS present, the isotope compositions of $Fe(II)_{aq}$ and $Fe(II)_{lib}$ are very similar, with the exception of the experiment with lepidocrocite at pH 8.6, where high concentrations of FeS relative to $Fe(II)_{aq}$ result in corrected $\delta^{56}Fe_{Fe(II)lib}$ values that are ~0.7 ‰ to 0.8 ‰ lower than the measured $\delta^{56}Fe_{Fe(II)aq}$ values (cf. Tables 2 and 4). However, as mentioned above, Wu et al., (2012a) showed that isotope exchange between $Fe(II)_{aq}$ and FeS occurs more rapidly at higher pH, presumably due to a change in $Fe(II)_{aq}$ speciation, which is dominated by sulfide complexes rather than $Fe^{2+}_{(aq)}$. This implies that the lower limit derived from our calculation likely reflects an overestimation of the $\delta^{56}Fe_{Fe(II)lib}$ value in this case. Nevertheless, for the majority of experiments, minor variations in the assumed isotope composition of the precipitated FeS will not significantly alter either our calculations of absolute fractionations or our conclusions.

The difference in isotope composition between the $\delta^{56}Fe_{Fe(II)lib}$ pool and the remaining surface reduced Fe(II) pool represents the apparent fractionation during the dissolution step ($\Delta^{56}Fe_{Fe(II)lib-Fe(II)ox}$), irrespective of FeS precipitation. With the exception of one experiment (ferrihydrite at pH 8.5), isotope fractionation during the dissolution step exceeds isotope fractionation during the reduction step, with more negative $\Delta^{56}Fe_{Fe(II)lib-Fe(II)ox}$ values (Table 4, Fig. 4). In these cases, the dissolution step results in the release of Fe(II) that is isotopically lighter

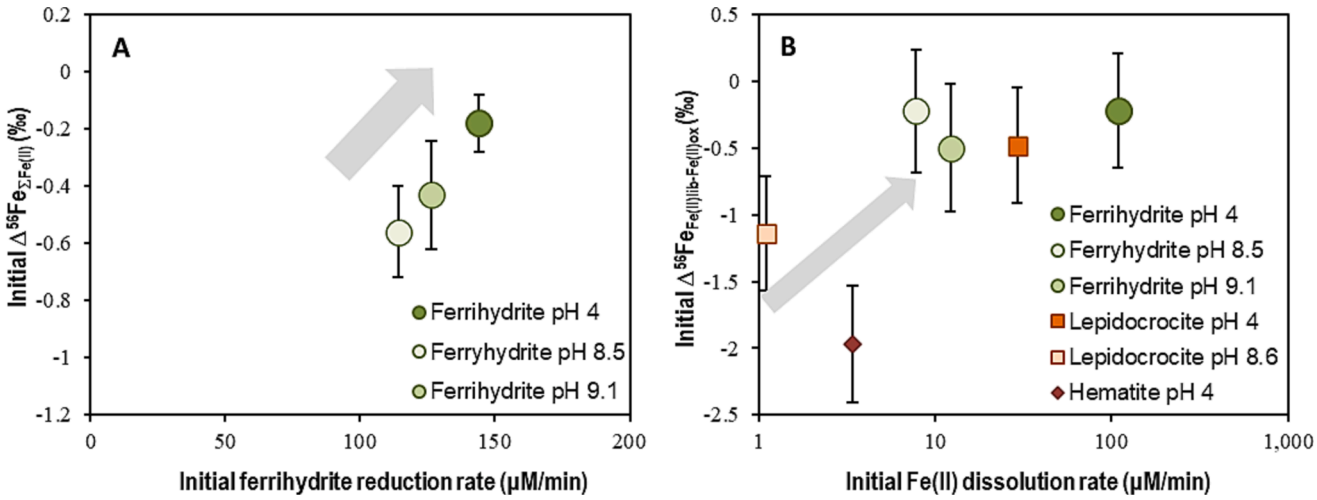

Fig. 6. Comparison of initial reaction rates for reduction (A) and dissolution (B) with their respective isotope fractionations for the reduction step ($\Delta^{56}Fe_{\Sigma Fe(II)-Fe\text{-}oxide}$) and dissolution step ($\Delta^{56}Fe_{Fe(II)lib-Fe(II)ox}$). Initial reaction rates and their average isotope fractionations were calculated for the linear phase of each experiment (see Fig. 2). Only ferrihydrite is considered for the reduction step, in order to highlight that for a particular mineral, it is the rate at which the oxide surface is reduced that initially controls the extent of fractionation. Note the log scale for the initial dissolution rate in Fig. 6B.

than that produced during the reduction step (Table 5), which is consistent with a significant body of evidence suggesting that reductive dissolution releases isotopically light Fe(II) to solution, regardless of the precise reductive mechanism (Beard et al., 1999; Brantley et al., 2004; Icopini et al., 2004; Crosby et al., 2005, 2007; Johnson et al., 2005; Wiederhold et al., 2006).

In determining the controls on isotope fractionation during this step, we again consider the influence of reaction rates. The rates of Fe(II) dissolution, as derived from the initial linear phase of the experiments (Fig. 2), show an overall increase between the isotope fractionations determined at slower and faster dissolution steps (Fig. 6B), suggesting that dissolution-step fractionations are controlled by dissolution rates, regardless of the precise mineralogy of the Fe-(oxyhydr)oxide. Dissolution rates are also strongly controlled by pH, with rates being faster at low pH (Pyzik and Sommer, 1981; Peiffer et al., 1992; Yao and Millero, 1996; Poulton, 2003) due to increased surface protonation, which causes a polarization and weakening of the metal–oxygen bonds (Zinder et al., 1986; Suter et al., 1991). Our experiments for individual minerals at different pH values show that average fractionations for the dissolution step increase at higher pH by ~0.2 to ~0.6 ‰ for both ferrihydrite and lepidocrocite, respectively (Fig. 6B), thus providing support for the dissolution rate control on isotopic fractionations proposed above. This inference of reaction rate control is consistent with observations by Crosby et al. (2007), who suggest that the magnitude of isotope fractionation is controlled by the rate of atom and electron transfer between the reactive Fe(II) and Fe(III) pools, and is independent of the nature of the ferric substrate.

5.2. Environmental and geological implications

Our data indicate that the reaction of dissolved sulfide with Fe (oxyhydr)oxide minerals clearly has the potential to generate light isotopic compositions in nature, with the dissolved phase (i.e., $Fe(II)_{lib}$) reaching isotope compositions up to ~ −0.8 ‰ (Table 4). This contrasts with previous assumptions that no fractionation would occur during this process (Johnson et al., 2004; Archer and Vance, 2006; Staubwasser et al., 2006). In fact, our experiments at different pH values suggest that $Fe(II)_{lib}$ fractionations for individual minerals increase as reaction rates decrease at higher pH (Table 4). Thus, with regard to the less reactive minerals such as hematite, we suggest that the $Fe(II)_{lib}$ fractionations of −0.65 to −0.75 ‰ observed at pH 4.0 (Table 4) may translate to significantly larger fractionations at the higher pH values characteristic of marine sediment porewaters.

The range of observed fractionations overlaps the lower end of experimental $\delta^{56}Fe$ fractionations reported during DIR, where aqueous phase compositions tend to be 0.5 to 2.3 ‰ lighter than the starting Fe (oxyhydr)oxide mineral (Beard et al., 1999; Icopini et al., 2004; Crosby et al., 2005, 2007; Johnson et al., 2005). In nature, however, marine sediment porewater $\delta^{56}Fe$ compositions tend to range from +0.4 to −3.4 ‰ (Severmann et al., 2006, 2010; Homoky et al., 2009, 2013). These porewater values reflect additional redox recycling and Fe^{2+} mobilization during diagenesis (Severmann et al., 2006; Homoky et al., 2013), highlighting that multiple cycling through both DIR and abiotic reduction with sulfide may lead to porewater $\delta^{56}Fe$ compositions significantly lower than those obtained experimentally.

The significant overlap between isotope fractionations generated during biological and abiological reductive dissolution highlights the difficulties inherent in distinguishing specific fractionation pathways in nature, which may be further complicated by isotope fractionation during the subsequent formation of iron sulfide minerals (Butler et al., 2005; Guilbaud et al., 2011a, b; Wu et al., 2012a; Mansor and Fantle, 2019; Heard et al., 2020). In fact, near the sediment–water interface in many organic-rich marine environments, DIR and sulfide-promoted reductive dissolution likely occur simultaneously, as the most reactive Fe minerals (e.g., ferrihydrite) are readily consumed via both processes (e.g. Canfield, 1989; Thamdrup, 2000; Krom et al., 2002; Roden, 2003; Poulton et al., 2004). In such environments, dissolved Fe^{2+} commonly accumulates in porewaters, and even though maximum rates of sulfate reduction commonly occur in this zone, dissolved sulfide is buffered to low concentrations through both the reaction with Fe (oxyhydr)oxides and through formation of FeS and pyrite (Canfield, 1989; Thamdrup, 2000; Krom et al., 2002). A combination of these processes may therefore contribute to the light dissolved Fe^{2+} isotope compositions commonly measured in the upper reaches of anoxic marine sediments (Severmann et al., 2006, 2010; Homoky et al., 2009). As the most reactive Fe minerals such as ferrihydrite are consumed with depth in the sediment profile, however, the less reactive minerals (e.g., goethite, hematite) still react on a relatively rapid timescale with the dissolved sulfide that builds up in porewaters (Canfield, 1989; Krom et al., 2002; Poulton et al., 2004). However, reduction of these Fe minerals by bacteria is very slow (Lovley and Phillips, 1988; Thamdrup, 2000) and thus in this zone, reduction by sulfide likely dominates. The Fe^{2+} released in this zone rapidly precipitates as sulfide minerals, the isotopic composition of which will be affected by fractionations imparted during both the

reductive dissolution process, and by Fe sulfide precipitation.

Sedimentary pyrite, the ultimate stable Fe sulfide in the environment, exhibits the largest range of δ^{56}Fe compositions in the rock record, from highly depleted values in pyritic shales (down to ~ −3.8 ‰; e.g., Rouxel et al., 2005) to highly enriched values in concentric nodules (up to ~ +4.1 ‰; Agangi et al., 2015). Experimental studies and natural observations have shown that pyrite formation pathways produce pyrite that is isotopically lighter than precursor Fe phases, and therefore the extent of sulfidation, together with the composition of the Fe source, play a significant role in the resulting pyrite-δ^{56}Fe composition (e.g., Guilbaud et al., 2011a; Virtasalo et al., 2013; Busigny et al., 2014; Scholz et al., 2014b; Lin et al., 2017; Rolison et al., 2018; Mansor and Fantle, 2019). Additionally, when isotopic equilibrium is achieved at higher temperatures (>300 °C), pyrite becomes ^{56}Fe-enriched, as predicted by theoretical calculations (Polyakov et al., 2007; Blanchard et al., 2009; Syverson et al., 2013). Yet, microbial processes such as DIR are largely invoked in the literature as the sole mechanism to explain ^{56}Fe-depleted signatures (e.g., Yamaguchi et al., 2005; Archer and Vance, 2006; Johnson et al., 2008b; Czaja et al., 2010; Nishizawa et al., 2010; Marin-Carbonne et al., 2014; Agangi et al., 2015; Yoshiya et al., 2015b, 2015a; Galić et al., 2017; Sawaki et al., 2018), whereas isotopically enriched pyrite is commonly attributed to the sulfidation of Fe (oxyhydr)oxide minerals (e.g., Whitehouse and Fedo, 2007; Nishizawa et al., 2010; Marin-Carbonne et al., 2014; Galić et al., 2017).

Quantitative sulfidation of ^{56}Fe-enriched Fe (oxyhydr)oxides would certainly result in pyrite that is mirroring the Fe isotope composition of the source. In this sense, our lepidocrocite experiments, with a large extent of reduction during sulfidation, demonstrate that the reduced solid products exhibit δ^{56}Fe compositions close to, or slightly heavier (~ +0.25 ‰) than the starting mineral. However, our results also clearly demonstrate that under typical marine and porewater pH, the sulfidation of more reactive phases such as ferrihydrite produces $Fe(II)_{solid}$ which can be ~ −0.6 ‰ lower than the starting mineral. This contrasts sharply with the recurrent assumption that the sulfidation of Fe (oxyhydr)oxides would produce an isotopically-enriched Fe precursor to pyrite.

6. Conclusions

Our experimental evaluation of the reaction between dissolved sulfide and Fe (oxyhydr)oxide minerals provides new insight into the generation of Fe isotope fractionations during abiotic reductive dissolution. Significant fractionations are evident during both the reductive step and the dissolution step of the reaction. For the reductive step, kinetic isotope fractionations of up to ~ −0.6 ‰ may be generated, while the dissolution step may produce $Fe(II)_{aq}$ down to ~ −0.8 ‰, with the magnitude of fractionation dependent on the nature of the Fe mineral and the processes controlling reaction rates.

Overall, our isotopic data suggest that fractionations of at least ~ −0.8 ‰ may be readily achieved in the dissolved phase through abiotic reductive dissolution mechanisms during marine sediment diagenesis, with the potential to generate significantly lighter isotope compositions through redox recycling of Fe. This suggests that in many organic-rich environments, a robust evaluation of the relative significance of DIR and sulfide-promoted reductive dissolution in the generation of Fe isotope fractionations may be nearly impossible to attain. In fact, in sulfidic sediments, the interaction of dissolved sulfide with Fe (oxyhydr)oxide minerals may ultimately be a dominant driver of Fe isotope fractionations, particularly as sediments are buried beneath the zone of bacterial Fe reduction. In such settings, the extent of isotopic fractionation will likely relate to the degree of redox recycling and the extent of reductive dissolution of the Fe (oxyhydr)oxide minerals present (through a combination of both DIR and sulfide-promoted reductive dissolution), with an additional fractionation factor related to the subsequent formation of Fe sulfide minerals. By contrast, DIR will likely be a dominant fractionation mechanism in sediments where sulfate reduction does not occur. These observations highlight the need for detailed geochemical analyses of biogeochemical redox cycling in the modern or ancient setting being studied, in order to allow a more rigorous interpretation of the Fe isotope signatures that are recorded.

CRediT authorship contribution statement

Alison McAnena: Formal analysis, Funding acquisition, Investigation, Visualization, Writing – original draft. **Silke Severmann:** Formal analysis, Resources. **Romain Guilbaud:** Writing – review & editing. **Simon W. Poulton:** Conceptualization, Funding acquisition, Methodology, Project administration, Resources, Supervision, Validation, Writing – review & editing.

Declaration of competing interest

The authors declare that they have no known competing financial interests or personal relationships that could have appeared to influence the work reported in this paper.

Acknowledgements

This work was funded by an EPSRC-DTA studentship awarded to AM. SWP acknowledges support from a Royal Society Wolfson Research Merit Award and Natural Environment Research Council grant NE/T006838/1, SS acknowledges support from US National Science Foundation grants OCE-0624704 and OPP-1029739. We are grateful for the constructive and supportive comments of the anonymous reviewers and Associate Editor Weiqiang Li, which significantly improved the final manuscript.

Appendix A. Supplementary material

Supplementary material includes a schematic of the experimental set-up, mineralogical data characterising the Fe minerals used in this study, and Phreeqc calculations for the dissolved species. Supplementary material to this article can be found online at https://doi.org/10.1016/j.gca.2024.01.032.

References

Agangi, A., Hofmann, A., Rollion-Bard, C., Marin-Carbonne, J., Cavalazzi, B., Large, R., Meffre, S., 2015. Gold accumulation in the Archaean Witwatersrand Basin, South Africa—Evidence from concentrically laminated pyrite. Earth Sci. Rev. 140, 27–53.
Amor, M., Busigny, V., Louvat, P., Gélabert, A., Cartigny, P., Durand-Dubief, M., Ona-Nguema, G., Alphandéry, E., Chebbi, I., Guyot, F., 2016. Mass-dependent and-independent signature of Fe isotopes in magnetotactic bacteria. Science 352, 705–708.
Anbar, A.D., 2004. Iron stable isotopes: beyond biosignatures. Earth Planet. Sci. Lett. 217, 223–236.
Archer, C., Vance, D., 2006. Coupled Fe and S isotope evidence for Archean microbial Fe (III) and sulfate reduction. Geology 34, 153–156.
Balci, N., Bullen, T.D., Witte-Lien, K., Shanks, W.C., Motelica, M., Mandernack, K.W., 2006. Iron isotope fractionation during microbially stimulated Fe(II) oxidation and Fe(III) precipitation. Geochim. Cosmochim. Acta 70, 622–639.
Beard, B.L., Johnson, C.M., Cox, L., Nealson, K.H., Aguilar, C., 1999. Iron isotope biosignatures. Science 285, 1889–1892.
Beard, B.L., Johnson, C.M., Skulan, J.L., Nealson, K.H., Cox, L., Sun, H., 2003. Application of Fe isotopes to tracing the geochemical and biological cycling of Fe. Chem. Geol. 195, 87–117.
Beard, B.L., Handler, R.M., Scherer, M.M., Wu, L., Czaja, A.D., Heimann, A., Johnson, C. M., 2010. Iron isotope fractionation between aqueous ferrous iron and goethite. Earth Planet. Sci. Lett. 295, 241–250.
Benning, L.G., Wilkin, R.T., Barnes, H.L., 2000. Reaction pathways in the Fe–S system below 100°C. Chem. Geol. 167, 25–51.
Berner, R.A., 1984. Sedimentary pyrite formation: an update. Geochim. Cosmochim. Acta 48, 605–615.
Blanchard, M., Poitrasson, F., Méheut, M., Lazzeri, M., Mauri, F., Balan, E., 2009. Iron isotope fractionation between pyrite (FeS_2), hematite (Fe_2O_3) and siderite ($FeCO_3$): a first-principles density functional theory study. Geochim. Cosmochim. Acta 73, 6565–6578.
Brantley, S.L., Liermann, L., Bullen, T.D., 2001. Fractionation of Fe isotopes by soil microbes and organic acids. Geology 29, 535–538.

Brantley, S.L., Liermann, L.J., Guynn, R.L., Anbar, A., Icopini, G.A., Barling, J., 2004. Fe isotopic fractionation during mineral dissolution with and without bacteria. Geochimica. Cosmochim. Acta 68, 3189–3204.
Bullen, T.D., White, A.F., Childs, C.W., Vivit, D.V., Schulz, M.S., 2001. Demonstration of significant abiotic ion isotope fractionation. Geology 29, 699–702.
Busigny, V., Planavsky, N.J., Jézéquel, D., Crowe, S., Louvat, P., Moureau, J., Viollier, E., Lyons, T.W., 2014. Iron isotopes in an Archean ocean analogue. Geochim. Cosmochim. Acta 133, 443–462.
Butler, I.B., Archer, C., Vance, D., Oldroyd, A., Rickard, D., 2005. Fe isotope fractionation on FeS formation in ambient aqueous solution. Earth and Planet Sci. Lett. 236.
Canfield, D.E., 1989. Reactive iron in marine sediments. Geochim. Cosmochim. Acta 53, 619–632.
Chanda, P., Amenabar, M.J., Boyd, E.S., Beard, B.L., Johnson, C.M., 2021. Stable Fe isotope fractionation during dissimilatory Fe(III) reduction by a thermoacidophile in acidic hydrothermal environments. Geochim. Cosmochim. Acta 292, 427–451.
Chapman, J.B., Weiss, D.J., Shan, Y., Lemburger, M., 2009. Iron isotope fractionation during leaching of granite and basalt by hydrochloric and oxalic acids. Geochim. Cosmochim. Acta 73, 1312–1324.
Cline, J.D., 1969. Spectrophotometric determination of hydrogen sulfide in natural waters. Limnol. Oceanogr. 14, 454–458.
Croal, L.R., Johnson, C.M., Beard, B.L., Newman, D.K., 2004. Iron isotope fractionation by Fe(II)-oxidizing photoautotrophic bacteria. Geochim Cosmochim Acta 68, 1127–1242.
Crosby, H.A., Johnson, C.M., Roden, E.E., Beard, B.L., 2005. Coupled Fe(II)-Fe(III) electron and atom exchange as a mechanism for Fe isotope fractionation during dissimilatory iron oxide reduction. Environ. Sci. Technol. 39, 6698–6704.
Crosby, H.A., Roden, E.E., Johnson, C., Beard, B.L., 2007. The mechanisms of iron isotope fractionation produced during dissimilatory Fe(III) reduction by Shewanella putrefaciens and Geobacter sulfurreducens. Geobiology 5, 169–189.
Czaja, A.D., Johnson, C.M., Beard, B.L., Eigenbrode, J.L., Freeman, K.H., Yamaguchi, K. E., 2010. Iron and carbon isotope evidence for ecosystem and environmental diversity in the ~ 2.7 to 2.5 Ga Hamersley Province, Western Australia. Earth Planet. Sci. Lett. 292, 170–180.
Czaja, A.D., Johnson, C.M., Yamaguchi, K.E., Beard, B.L., 2012. Comment on "Abiotic pyrite formation produces a large Fe isotope fractionation". Science 335, 538.
Dauphas, N., Rouxel, O., 2006. Mass Spectrometry and natural variations of iron isotopes. Mass Spectrom. Rev. 25, 515–550.
Dos Santos, A.M., Stumm, W., 1992. Reductive dissolution of iron (III)(hydr) oxides by hydrogen sulfide. Langmuir 8, 1671–1675.
Drever, J., Stillings, L., 1997. The role of organic acids in mineral weathering. Colloids Surf. A Physicochem. Eng. Asp 120, 167–181.
Dupeyron, J., Decraene, M.-N., Marin-Carbonne, J., Busigny, V., 2023. Formation pathways of Precambrian sedimentary pyrite: Insights from in situ Fe isotopes. Earth Planet. Sci. Lett. 609, 118070.
Fantle, M.S., DePaolo, D.J., 2004. Iron isotopic fractionation during continental weathering. Earth and Planet. Sci. Lett. 228, 547–562.
Frierdich, A.J., Beard, B.L., Scherer, M.M., Johnson, C.M., 2014. Determination of the Fe (II) aq–magnetite equilibrium iron isotope fractionation factor using the three-isotope method and a multi-direction approach to equilibrium. Earth Planet. Sci. Lett. 391, 77–86.
Galić, A., Mason, P.R., Mogollón, J.M., Wolthers, M., Vroon, P.Z., Whitehouse, M.J., 2017. Pyrite in a sulfate-poor Paleoarchean basin was derived predominantly from elemental sulfur: evidence from 3.2 Ga sediments in the Barberton Greenstone Belt, Kaapvaal Craton. Chem. Geol. 449, 135–146.
Guilbaud, R., Butler, I.B., Ellam, R.M., Rickard, D., 2010. Fe isotope exchange between Fe $(II)_{aq}$ and nanoparticulate mackinawite (FeS_m) during nanoparticle growth. Earth Planet. Sci. Lett. 300, 174–183.
Guilbaud, R., Butler, I.B., Ellam, R.M., 2011a. Abiotic pyrite formation produces a large Fe isotope fractionation. Science 332, 1548–1551.
Guilbaud, R., Butler, I.B., Ellam, R.M., Rickard, D., Oldroyd, A., 2011b. Experimental determination of the equilibrium Fe isotope fractionation between and FeS_m (mackinawite) at 25 and 2 °C. Geochim. Cosmochim. Acta 75, 2721–2734.
Guilbaud, R., Butler, I.B., Ellam, R.M., 2012. Response to Comment on "Abiotic pyrite formation produces a large Fe isotope fractionation". Science 335, 538.
Handler, R.M., Beard, B.L., Johnson, C.M., Scherer, M.M., 2009. Atom exchange between aqueous Fe(II) and goethite: an Fe isotope tracer study. Environ. Sci. Tech. 43, 1102–1107.
Heard, A.W., Dauphas, N., Guilbaud, R., Rouxel, O.J., Butler, I.B., Nie, N.X., Bekker, A., 2020. Triple iron isotope constraints on the role of ocean iron sinks in early atmospheric oxygenation. Science 370, 446–449.
Hellige, K., Pollok, K., Larese-Casanova, P., Behrends, T., Peiffer, S., 2012. Pathways of ferrous iron mineral formation upon sulfidation of lepidocrocite surfaces. Geochim. Cosmochim. Acta 81, 69–81.
Homoky, W.B., Severmann, S., Mills, R.A., Statham, P.J., Fones, G.R., 2009. Pore-fluid Fe isotopes reflect the extent of benthic Fe redox recycling: evidence from continental shelf and deep-sea sediments. Geology 37, 751–754.
Homoky, W.B., John, S.G., Conway, T.M., Mills, R.A., 2013. Distinct iron isotopic signatures and supply from marine sediment dissolution. Nat. Commun. 4, 1–10.
Icopini, G.A., Anbar, A.D., Ruebush, S.S., Tien, M., Brantley, S.L., 2004. Iron isotope fractionation during microbial reduction of iron: The importance of adsorption. Geology 32, 205–208.
Ilina, S.M., Poitrasson, F., Lapitskiy, S.A., Alekhin, Y.V., Viers, J., Pokrovsky, O.S., 2013. Extreme iron isotope fractionation between colloids and particles of boreal and temperate organic-rich waters. Geochim. Cosmochim. Acta 101, 96–111.
Johnson, C.M., Skulan, J.L., Beard, B.L., Sun, H., Nealson, K.H., Braterman, P.S., 2002. Isotopic fractionation between Fe(III) and Fe(II) in aqueous solutions. Earth Planet. Sci. Lett. 195, 141–153.
Johnson, C.M., Beard, B.L., Roden, E.E., Newman, D.K., Nealson, K.H., 2004. Isotopic constraints on biochemical cycling of Fe. Rev. Mineral. Geochem. 55, 359–408.
Johnson, C.M., Beard, B.L., Welch, S., Croal, L., Newman, D., Nealson, K., 2005. Experimental constraints on Fe isotope fractionations during biogeochemical cycling of Fe. Geochim. Cosmochim. Acta 66, A371.
Johnson, C.M., Beard, B.L., Klein, C., Beukes, N.J., Roden, E.E., 2008a. Iron isotopes constrain biologic and abiologic processes in banded iron formation genesis. Geochim Cosmochim Acta 72, 151–169.
Johnson, C.M., Beard, B.L., Roden, E.E., 2008b. The iron isotope fingerprints of redox and biogeochemical cycling in modern and ancient Earth. Annu. Rev. Earth Planet. Sci. 36, 457–493.
Kappler, A., Johnson, C., Crosby, H., Beard, B., Newman, D., 2010. Evidence for equilibrium iron isotope fractionation by nitrate-reducing iron (II)-oxidizing bacteria. Geochim. Cosmochim. Acta 74, 2826–2842.
Kiczka, M., Wiederhold, J.G., Frommer, J., Kraemer, S.M., Bourdon, B., Kretzschmar, R., 2010. Iron isotope fractionation during proton-and ligand-promoted dissolution of primary phyllosilicates. Geochim. Cosmochim. Acta 74, 3112–3128.
Krom, M.D., Mortimer, R.J., Poulton, S.W., Hayes, P., Davies, I.M., Davison, W., Zhang, H., 2002. In-situ determination of dissolved iron production in recent marine sediments. Aquat. Sci. 64, 282–291.
Liermann, L.J., Mathur, R., Wasylenki, L.E., Nuester, J., Anbar, A.D., Brantley, S.L., 2011. Extent and isotopic composition of Fe and Mo release from two Pennsylvania shales in the presence of organic ligands and bacteria. Chem. Geol. 281, 167–180.
Lin, Z., Sun, X., Lu, Y., Strauss, H., Xu, L., Gong, J., Teichert, B.M., Lu, R., Lu, H., Sun, W., 2017. The enrichment of heavy iron isotopes in authigenic pyrite as a possible indicator of sulfate-driven anaerobic oxidation of methane: Insights from the South China Sea. Chem. Geol. 449, 15–29.
Lovley, D.R., Phillips, E.J., 1988. Novel mode of microbial energy metabolism: organic carbon oxidation coupled to dissimilatory reduction of iron or manganese. Appl. Environ. Microbiol. 54, 1472–1480.
Mansor, M., Fantle, M.S., 2019. A novel framework for interpreting pyrite-based Fe isotope records of the past. Geochim. Cosmochim. Acta.
Marin-Carbonne, J., Rollion-Bard, C., Bekker, A., Rouxel, O., Agangi, A., Cavalazzi, B., Wohlgemuth-Ueberwasser, C.C., Hofmann, A., McKeegan, K.D., 2014. Coupled Fe and S isotope variations in pyrite nodules from Archean shale. Earth Planet. Sci. Lett. 392, 67–79.
Maters, E.C., Mulholland, D.S., Flament, P., de Jong, J., Mattielli, N., Deboudt, K., Dhont, G., Bychkov, E., 2022. Laboratory study of iron isotope fractionation during dissolution of mineral dust and industrial ash in simulated cloud water. Chemosphere 299, 134472.
Matthews, A., Zhu, X.K., O'Nions, K., 2001. Kinetic iron stable isotope fractionation between iron (-II) and (-III) complexes in solution. Earth Planet Sci. Lett. 192.
Michel, F.M., Ehm, L., Antao, S.M., Lee, P.L., Chupas, P.J., Liu, G., Strongin, D.R., Schoonen, M.A.A., Phillips, B.L., Parise, J.B., 2007. The structure of ferrihydrite, a nanocrystalline material. Science 316, 1726–1729.
Mikutta, C., Wiederhold, J.G., Cirpka, O.A., Hofstetter, T.B., Bourdon, B., Gunten, U.V., 2009. Iron isotope fractionation and atom exchange during sorption of ferrous iron to mineral surfaces. Geochim. Cosmochim. Acta 73, 1795–1812.
Mulholland, D.S., Flament, P., de Jong, J., Mattielli, N., Deboudt, K., Dhont, G., Bychkov, E., 2021. In-cloud processing as a possible source of isotopically light iron from anthropogenic aerosols: New insights from a laboratory study. Atmos. Environ. 259, 118505.
Nishizawa, M., Yamamoto, H., Ueno, Y., Tsuruoka, S., Shibuya, T., Sawaki, Y., Yamamoto, S., Kon, Y., Kitajima, K., Komiya, T., Maruyama, S., Hirata, T., 2010. Grain-scale iron isotopic distribution of pyrite from Precambrian shallow marine carbonate revealed by a femtosecond laser ablation multicollector ICP-MS technique: possible proxy for the redox state of ancient seawater. Geochim. Cosmochim. Acta 74, 2760–2778.
Oleinikova, O.V., Poitrasson, F., Drozdova, O.Y., Shirokova, L.S., Lapitskiy, S.A., Pokrovsky, O.S., 2019. Iron isotope fractionation during bio-and photodegradation of organoferric colloids in boreal humic waters. Environ. Sci. Tech. 53, 11183–11194.
Opfergelt, S., Williams, H.M., Cornelis, J.T., Guicharnaud, R.A., Georg, R.B., Siebert, C., Gislason, S.R., Halliday, A.N., Burton, K.W., 2017. Iron and silicon isotope behaviour accompanying weathering in Icelandic soils, and the implications for iron export from peatlands. Geochim. Cosmochim. Acta 217, 273–291.
Ostrander, C.M., Severmann, S., Gordon, G.W., Kendall, B., Lyons, T.W., Zheng, W., Roy, M., Anbar, A.D., 2022. Significance of 56Fe depletions in late-Archean shales and pyrite. Geochim. Cosmochim. Acta 316, 87–104.
Peiffer, S., Dos Santos Afonso, M., Wehrli, B., Gaechter, R., 1992. Kinetics and mechanism of the reaction of hydrogen sulfide with lepidocrocite. Environ. Sci. Tech. 26, 2408–2413.
Peiffer, S., Gade, W., 2007. Reactivity of ferric oxides toward H_2S at low pH. Environ. Sci. Tech. 41, 3159–3164.
Polyakov, V.B., Clayton, R.N., Horita, J., Mineev, S.D., 2007. Equilibrium iron isotope fractionation factors of minerals: reevaluation from the data of nuclear inelastic resonant X-ray scattering and Mössbauer spectroscopy. Geochim. Cosmochim. Acta 71, 3833–3846.
Poulson, R.L., Johnson, C.M., Beard, B.L., 2005. Iron isotope exchange kinetics at the nanoparticulate ferrihydrite surface. Am. Mineral. 90, 758–763.
Poulton, S.W., 2003. Sulfide oxidation and iron dissolution kinetics during the reaction of dissolved sulfide with ferrihydrite. Chem. Geol. 202, 79–94.

Poulton, S.W., Krom, M.D., Raiswell, R., 2004. A revised scheme for the reactivity of iron (oxyhydr) oxide minerals towards dissolved sulfide. Geochim. Cosmochim. Acta 68, 3703–3715.
Pyzik, A.J., Sommer, S.E., 1981. Sedimentary iron monosulfides: kinetics and mechanisms of formation. Geochim. Cosmochim Acta 45.
Qi, M., Gao, T., Wang, Z., Yuhui, L., Xia, Y., Song, C., Yizhang, L., Liu, C., 2022. Iron solid-phase differentiation controls isotopic fractionation during lateritic weathering of basalt. Catena 217, 106512.
Rickard, D., 1974. Kinetics and mechanisms of the sulfidation of goethite. Am. J. Sci. 274, 941–952.
Rickard, D., 1995. Kinetics of FeS precipitation: Part 1. Competing reaction mechanisms. Geochim. Cosmochim. Acta 59, 4367–4379.
Rickard, D., 2006. The solubility of FeS. Geochim. Cosmochim. Acta 70, 5779–5789.
Rickard, D., Morse, J.W., 2005. Acid Volatile Sulfide (AVS). Mar. Chem. 97, 141–197.
Roden, E.E., 2003. Fe (III) oxide reactivity toward biological versus chemical reduction. Environ. Sci. Tech. 37, 1319–1324.
Rolison, J.M., Stirling, C.H., Middag, R., Gault-Ringold, M., George, E., Rijkenberg, M.J., 2018. Iron isotope fractionation during pyrite formation in a sulfidic Precambrian ocean analogue. Earth Planet. Sci. Lett. 488, 1–13.
Rouxel, O.J., Bekker, A., Edwards, K.J., 2005. Iron isotope constraints on the Archean and Paleoproterozoic ocean redox state. Science 307, 1088–1090.
Rouxel, O., Sholkovitz, E., Charette, M., Edwards, K.J., 2008. Iron isotope fractionation in subterranean estuaries. Geochim. Cosmochim. Acta 72, 3413–3430.
Roy, M., Rouxel, O., Martin, J.B., Cable, J.E., 2012. Iron isotope fractionation in a sulfide-bearing subterranean estuary and its potential influence on oceanic Fe isotope flux. Chem. Geol. 300, 133–142.
Sawaki, Y., Tahata, M., Komiya, T., Hirata, T., Han, J., Shu, D., 2018. Redox history of the Three Gorges region during the Ediacaran and Early Cambrian as indicated by the Fe isotope. Geosci. Front. 9, 155–172.
Scholz, F., Severmann, S., McManus, J., Hensen, C., 2014a. Beyond the Black Sea paradigm: the sedimentary fingerprint of an open-marine iron shuttle. Geochim. Cosmochim. Acta 127, 368–380.
Scholz, F., Severmann, S., McManus, J., Noffke, A., Lomnitz, U., Hensen, C., 2014b. On the isotope composition of reactive iron in marine sediments: Redox shuttle versus early diagenesis. Chem. Geol. 389, 48–59.
Schwertmann, U., Cornell, R., 1991. Preparation and characterization. In: Iron oxides in the laboratory, 64.
Severmann, S., Johnson, C.M., Beard, B.L., McManus, J., 2006. The effect of early diagenesis on the Fe isotope compositions of porewaters and authigenic minerals in continental margin sediments. Geochim Cosmochim Acta 70, 2006–2022.
Severmann, S., McManus, J., Berelson, W.M., Hammond, D.E., 2010. The continental shelf benthic iron flux and its isotope composition. Geochim. Cosmochim. Acta 74, 3984–4004.
Silvester, E., Charlet, L., Tournassat, C., Géhin, A., Grenèche, J.-M., Liger, E., 2005. Redox potential measurements and Mössbauer spectrometry of FeII adsorbed onto FeIII (oxyhydr) oxides. Geochim. Cosmochim. Acta 69, 4801–4815.
Skulan, J.L., Beard, B.L., Johnson, C.M., 2002. Kinetic and equilibrium Fe isotope fractionation between aqueous Fe(III) and hematite. Geochim. Cosmochim. Acta 66, 2995–3015.
Staubwasser, M., von Blanckenburg, F., Schoenberg, R., 2006. Iron isotopes in the early marine diagenetic iron cycle. Geology 34, 629–632.
Suter, D., Banwart, S., Stumm, W., 1991. Dissolution of hydrous iron (III) oxides by reductive mechanisms. Langmuir 7, 809–813.
Syverson, D.D., Borrok, D.M., Seyfried Jr, W.E., 2013. Experimental determination of equilibrium Fe isotopic fractionation between pyrite and dissolved Fe under hydrothermal conditions. Geochim. Cosmochim. Acta 122, 170–183.
Tangalos, G., Beard, B., Johnson, C., Alpers, C.N., Shelobolina, E., Xu, H., Konishi, H., Roden, E., 2010. Microbial production of isotopically light iron (II) in a modern chemically precipitated sediment and implications for isotopic variations in ancient rocks. Geobiology 8, 197–208.
Teutsch, N., von Gunten, U., Porcelli, D., Cirpka, O.A., Halliday, A.N., 2005. Adsorption as a cause for iron isotope fractionation in reduced groundwater. Geochim Cosmochim Acta 69, 4175–4185.
Thamdrup, B., 2000. Bacterial manganese and iron reduction in aquatic sediments. In: Advances in microbial ecology, Springer, pp. 41–84.
Viollier, E., Inglett, P., Hunter, K., Roychoudhury, A., Van Cappellen, P., 2000. The ferrozine method revisited: Fe (II)/Fe (III) determination in natural waters. Appl. Geochem. 15, 785–790.
Virtasalo, J.J., Whitehouse, M.J., Kotilainen, A.T., 2013. Iron isotope heterogeneity in pyrite fillings of Holocene worm burrows. Geology 41, 39–42.
Wan, M., Shchukarev, A., Lohmayer, R., Planer-Friedrich, B., Peiffer, S., 2014. Occurrence of surface polysulfides during the interaction between ferric (hydr) oxides and aqueous sulfide. Environ. Sci. Tech. 48, 5076–5084.
Welch, S.A., Beard, B.L., Johnson, C.M., Baterman, P.S., 2003. Kinetic and equilibrium Fe isotope fractionation between aqueous Fe(II) and Fe(III). Geochim. Cosmochim. Acta 67, 4231–4250.
Whitehouse, M.J., Fedo, C.M., 2007. Microscale heterogeneity of Fe isotopes in >3.71 Ga banded iron formation from the Isua Greenstone Belt, southwest Greenland. Geology 35, 719–722.
Wiederhold, J.G., Kraemer, S.M., Teutsch, N., Borer, P.M., Halliday, A.N., Kretzschmar, R., 2006. Iron isotope fractionation during proton-promoted, ligand-controlled, and reductive dissolution of goethite. Environ. Sci. Tech. 40, 3787–3793.
Wiesli, R.A., Beard, B.L., Johnson, C.M., 2004. Experimental determination of Fe isotope fractionation between aqueous Fe(II), siderite and “green rust” in abiotic systems. Chem. Geol. 211, 343–362.
Wolfe, A.L., Stewart, B.W., Capo, R.C., Liu, R., Dzombak, D.A., Gordon, G.W., Anbar, A. D., 2016. Iron isotope investigation of hydrothermal and sedimentary pyrite and their aqueous dissolution products. Chem. Geol. 427, 73–82.
Wolthers, M., van der Gaast, S.J., Charlet, L., Rickard, D., 2005. A surface and structural model describing the environmental reactivity of disordered mackinawite. Am. Mineral. 88, 2007–2015.
Wu, L., Beard, B.L., Roden, E.E., Johnson, C.M., 2009. Influence of pH and dissolved Si on Fe isotope fractionation during dissimilatory microbial reduction of hematite. Geochim. Cosmochim. Acta 73, 5584–5599.
Wu, L., Beard, B.L., Roden, E.E., Johnson, C.M., 2011. Stable iron isotope fractionation between aqueous Fe (II) and hydrous ferric oxide. Environ. Sci. Tech. 45, 1847–1852.
Wu, L., Druschel, G., Findlay, A., Beard, B.L., Johnson, C.M., 2012a. Experimental determination of iron isotope fractionations among Fe^{2+}_{aq}–FeS_{aq-} Mackinawite at low temperatures: implications for the rock record. Geochim. Cosmochim. Acta 89, 46–61.
Wu, L., Percak-Dennett, E.M., Beard, B.L., Roden, E.E., Johnson, C.M., 2012b. Stable iron isotope fractionation between aqueous Fe (II) and model Archean ocean Fe–Si coprecipitates and implications for iron isotope variations in the ancient rock record. Geochim. Cosmochim. Acta 84, 14–28.
Yamaguchi, K.E., Johnson, C.M., Beard, B.L., Ohmoto, H., 2005. Biogeochemical cycling of iron in the Archean-Paleoproterozoic Earth: Constraints from iron isotope variations in sedimentary rocks from the Kaapvaal and Pilbara Cratons. Chem. Geol. 218, 135–169.
Yanina, S.V., Rosso, K.M., 2008. GEOC 21-Redox transformation of hematite mediated by biased bulk crystal conduction. In: Abstracts of Papers of the American Chemical Society. AMER Chemical Soc 1155 16th ST, NW, WASHINGTON, DC 20036 USA.
Yao, W., Millero, F.J., 1996. Oxidation of hydrogen sulfide by hydrous Fe (III) oxides in seawater. Mar. Chem. 52, 1–16.
Yoshiya, K., Sawaki, Y., Hirata, T., Maruyama, S., Komiya, T., 2015a. In-situ iron isotope analysis of pyrites in~ 3.7 Ga sedimentary protoliths from the Isua supracrustal belt, southern West Greenland. Chem. Geol. 401, 126–139.
Yoshiya, K., Sawaki, Y., Shibuya, T., Yamamoto, S., Komiya, T., Hirata, T., Maruyama, S., 2015b. In-situ iron isotope analyses of pyrites from 3.5 to 3.2 Ga sedimentary rocks of the Barberton Greenstone Belt, Kaapvaal Craton. Chem. Geol. 403, 58–73.
Zinder, B., Furrer, G., Stumm, W., 1986. The coordination chemistry of weathering: II. Dissolution of Fe (III) oxides. Geochim. Cosmochim. Acta 50, 1861–1869.